Journal of Inorganic Biochemistry 236 (2022) 111977

Contents lists available at ScienceDirect

Journal of Inorganic Biochemistry

journal homepage: www.elsevier.com/locate/jinorgbio

Light activation of iridium(III) complexes driving ROS production and DNA damage enhances anticancer activity in A549 cells

Wenlong Li [a], Chuanling Shi [a], Xiaoyun Wu [a], Yuanyuan Zhang [a], Haimei Liu [a], Xiuzhen Wang [a,*], Chunxia Huang [a], Lijuan Liang [a], Yunjun Liu [a,b,**]

[a] School of Pharmacy, Guangdong Pharmaceutical University, Guangzhou 510006, PR China
[b] Guangdong Provincial Key Laboratory of Advanced Drug Delivery Systems and Guangdong Provincial Engineering Center of Topical Precise Drug Delivery System, Guangdong Pharmaceutical University, Guangzhou 510006, PR China

ARTICLE INFO

Keywords:
Iridium(III) complexes
Photoactivation
Apoptosis
Immunogenic cell death
Mitochondria

ABSTRACT

The work aimed to synthesize and characterize two iridium(III) complexes $[Ir(ppy)_2(IPPH)](PF_6)$ (**Ir1**, IPPH = (2*S*,3*R*,5*S*,6*R*)-2-(2-(1*H*-imidazo[4,5-*f*][1,10]phenanthrolin-2-yl)phenoxy)-6-(hydroxymethyl)tetrahydro-2*H*-pyran-3,4,5-triol, ppy = 2-phenylpyridine), $[Ir(piq)_2(IPPH)](PF_6)$ (**Ir2**, piq = 1-phenylisoquinoline). The cytotoxicity of the complexes against BEL-7402, A549, HCT-116, B16 cancer cells and normal LO2 was evaluated through 3-(4,5-dimethylthiazole-2-yl)-2,5-biphenyl tetrazolium bromide (MTT) method. The complexes show no cytotoxic activity ($IC_{50} > 100$ μM) against these cancer cells, while their cytotoxicity can significantly be elevated upon illumination. The IC_{50} values range from 0.2 ± 0.05 to 35.5 ± 3.5 μM. The cellular uptake, endoplasmic reticulum and mitochondria localization, reactive oxygen species, the change of mitochondrial membrane potential, γ-H2AX levels, cycle arrest, apoptosis and the expression of B-cell lymphoma-2 were investigated. The calreticulin (CRT), heat shock protein 70 (HSP70), high mobility group box 1 (HMGB1) were explored. This study demonstrates that photoactivatable complexes induce cell death in A549 through ROS-mediated endoplasmic reticulum stress-mitochondrial pathway, DNA damage pathways, immunogenic cell death (ICD), activation of PI3K/AKT signaling pathway and inhibit the cell growth at S phase.

1. Introduction

Cancer remains one of the most challenging and dangerous health burden for human beings worldwide [1]. The main cause of cancer-related death is not the tumor itself but the metastasis from the tumor [2]. Since the discovery of cisplatin by Rosenberg in the 1960s, the efficacy of platinum drugs in cancer chemotherapy has been limited by side effects such as drug resistance, neurotoxicity, nephrotoxicity,

Abbreviations: A549, human non-small cell lung cancer cells; ATP, adenosine triphosphate; AKT, protein kinase B; B16, mouse melanoma cells; Bax, Bcl-2 associated x protein; BCA, bicinchoninic acid; Bcl-2, B-cell lymphoma-2; BEL-7402, human hepatocarcinoma cells; Caspase-3, cysteinyl aspartate specific proteinase-3; CCCP, carbonyl cyanide *m*-chlorophenyl hydrazone; CRT, calreticulin; DAPI, 4′,6-Diamidino-2-phenylindole; DCF, 2′,7’-Dichlorofluorescein; DCHF, 2′,7’-Dichlorodihydrofluorescein; DCHF-DA, 2′,7’-Dichlorodihydrofluorescein diacetate; DMEM, Dulbecco's Modified Eagle Medium; DMSO, dimethylsulfoxide; EDTA, ethylene diamine tetraacetic acid; FBS, fetal bovine serum; FITC, fluorescein isothiocyanate; HCT-116, human colorectal carcinoma cells; HeLa, human cervical cancer cells; HepG2, human-hepatocarcinoma cells; HMGB1, high mobility group box1; HSP70, heat shock protein 70; ICD, immunogenic cell death; IPPH, (2*S*,3*R*,5*S*,6*R*)-2-(2-(1*H*-imidazo[4,5-*f*][1,10]phenanthrolin-2-yl)phenoxy)-6-(hydroxymethyl)tetrahydro-2*H*-pyran-3,4,5-triol; JC-1, 5,5′-6,6′-tetrachloro-1,1′-3,3′-tetrethylbenzimidalylcarbocyanine iodide; LED, light emitting diode; LO2, human normal liver cells; MDA, malondialdehyde; MMP, mitochondrial membrane potential; MTT, 3-(4,5-dimethylthiazole-2-yl)-2,5-biphenyl tetrazolium bromide; NBCS, Newborn calf serum; PARP, poly ADP-ribose polymerase; PBS, phosphate buffer solution; PDT, photodynamic therapy; PI, propidium iodide; PI3K, phosphatidylinositol 3-kinase; piq, 1-phenylisoquinoline; PMSF, phenylmethylsulfonyl fluoride; Hppy, 2-phenylpyridine; PVDF, polyvinylidene difluoride; RIPA, 50 mM Tris (pH 7.4), 150 mM NaCl, 1% NP-40, 0.5% sodium deoxycholate; RLU, Relative luminometer units; RNase, ribonuclease; ROS, reactive oxygen species; RPMI 1640, Roswell Park Memorial Institute 1640; SDS-PAGE, sodium dodecyl sulfate polyacrylamide gel electrophoresis; TBA, thiobarbituric acid; TBST 20, mM Tris–HCl, 150 mM NaCl, 0.2% Tween 20; TMS, tetramethylsilane; Tris, Tris(hydroxymethyl)aminomethane; Tween 20, polysorbate 20.

* Corresponding author.
** Corresponding author at: School of Pharmacy, Guangdong Pharmaceutical University, Guangzhou 510006, PR China.
E-mail addresses: wxzqq1234@gdpu.edu.cn (X. Wang), lyjche@gdpu.edu.cn (Y. Liu).

https://doi.org/10.1016/j.jinorgbio.2022.111977
Received 25 July 2022; Received in revised form 10 August 2022; Accepted 19 August 2022
Available online 23 August 2022

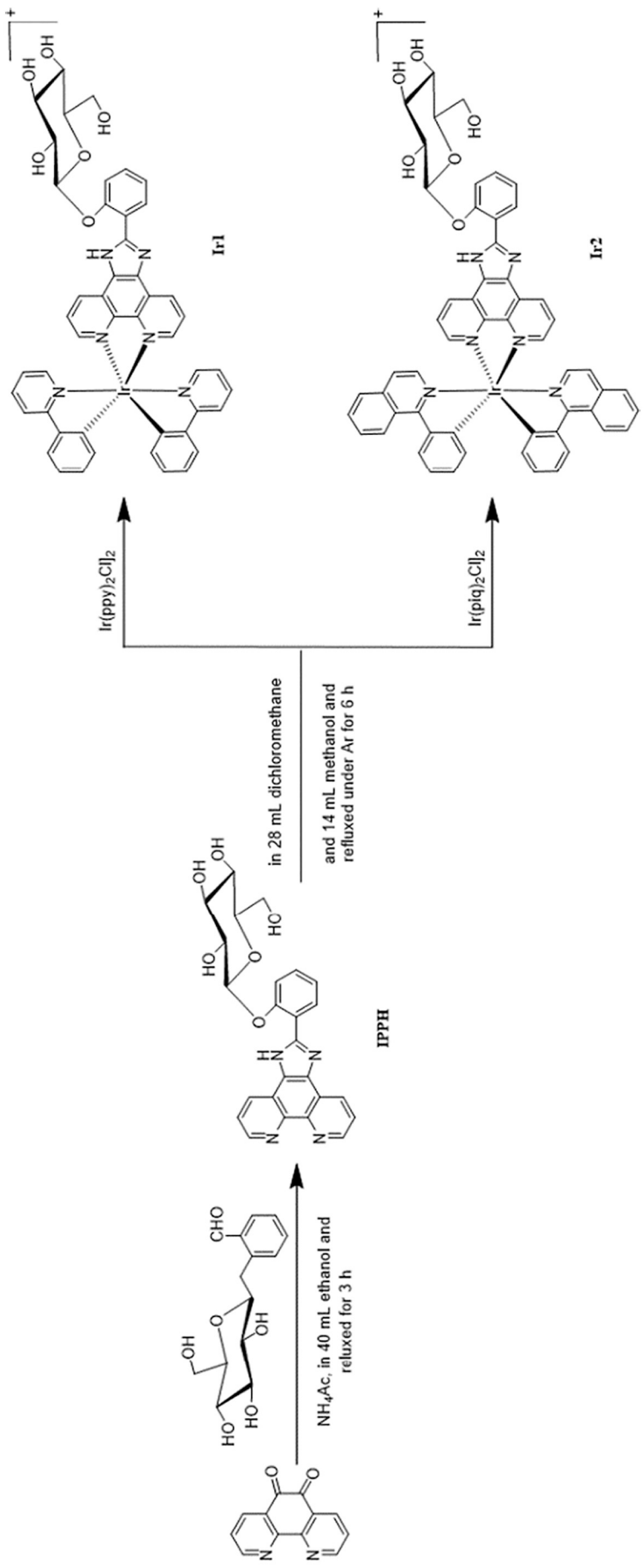

Scheme 1. Synthetic route for ligand and its complexes **Ir1** and **Ir2**

hepatotoxicity and selectivity of treatment [3–6]. Unfortunately, the resistance and toxic side effects associated with chemotherapy, radiotherapy and surgery make cancer treatment troublesome [7]. Photodynamic therapy (PDT) has attracted great attention for its high efficiency, low side effects and overcoming drug resistance compared to traditional cancer treatment strategies [8–10]. In PDT, the photosensitizer is activated by light and the excited triplet state of the photosensitizer converts the ground state $^3O_2$ into the active singlet oxygen ($^1O_2$) which kills cancer cells (type II reactions). The Radical species such as superoxide ion (O_2^-) and hydroxyl radical (·OH) were formed by electron transfer reactions (type I reactions) [11–13].

In our early work, we found that a range of iridium(III) complexes have unique anticancer mechanisms, such as mitochondrial dysfunction, DNA binding, ROS elevation, immunogenic cell death, endoplasmic reticulum stress, the release of cytochrome *c* [14–18]. Encouragingly, iridium(III) complexes are extensively investigated as showing great potential for photocatalytic cancer therapy in the field of photodynamic therapy (PDT) agent [19–33]. Glucose is essential to mammalian cells because it is not only a precursor of glycoproteins, triglycerides, and glycogen but also a crucial energy source through the generation of adenosine triphosphate (ATP) [34–38], moreover, the iridium complexes containing glucose can increase cell uptake and show high anticancer activity [39]. To obtain much information on the anticancer activity, in this work, two new pending glucose iridium(III) complexes $[Ir(ppy)_2(IPPH)](PF_6)$ (**Ir1**, ppy = 2-phenylpyridine, IPPH = (2*S*,3*R*,5*S*,6*R*)-2-(2-(1*H*-imidazo[4,5-*f*][1,10]phenanthrolin-2-yl)phenoxy)-6- (hydroxymethyl)tetrahydro-2*H*-pyran-3,4,5-triol) and $[Ir(piq)_2(IPPH)](PF_6)$ (**Ir2**, piq = 1-phenylisoquinoline, Scheme 1) were designed, synthesized and characterized by HRMS, ^{1}H NMR and ^{13}C NMR. **Ir1** and **Ir2** showed no activity against selected BEL-7402 (human hepatocarcinoma cells), A549 (human lung cancer cells), HCT116 (human colon cells), B16 (mouse melanoma cells) and normal LO2 (human normal liver cells). However, the complexes were irradiated with a 65w LED lamp (white light, 5.2 *J* cm^{-2}, λ = 450–465 nm) for 40 min. **Ir1** and **Ir2** were highly photoactive in subduing cancer cells, especially on A549 cells. In addition, cytotoxicity, endoplasmic reticulum and mitochondria localization, apoptosis, intracellular ROS levels, the change of mitochondrial membrane potential, immunogenic cell death, the expression of B-cell lymphoma-2 (Bcl-2) family proteins were investigated in detail.

2. Experimental

2.1. Materials and methods

All chemical reagents were purchased and used directly without further purification. $IrCl_3{\cdot}3H_2O$ was obtained from the Kunming Boren Precious Metals Co., Ltd. 1,10-phenanthroline was obtained from the Guangzhou Chemical Reagent Factory. Fetal Bovine Serum (FBS) and Newborn Calf Serum (NBCS) were purchased from Gibco company. Dulbecco's Modified Eagle Medium (DMEM) and Roswell Park Memorial Institute (RPMI) 1640 were purchased from Thermo Fisher Scientific (Waltham, USA). The tumor cell lines BEL-7402, A549, HCT116, B16 cancer cells and normal LO2 were gained from the Cell Center of Sun Yat-Sen University (Guangzhou, China). 3-(4,5-dimethyl-tiazol-2-ly)-2,5-diphenyl-tetrazoliumbromide (MTT) was purchased from Shanghai Beyotime Institute of Biotechnology (Shanghai, China). 2′,7′-dichlorodihydrofluorescein diacetate (DCFH-DA) and 5,5′-6,6′-tetrachloro-1,1′-3,3′-tetrethylbenzimidalylcarbocyanine iodide (JC-1) were purchased from Roche Diagnostics (Indianapolis, IN, USA). ^{1}H and ^{13}C NMR spectra were recorded on a Varian-500 spectrometer with DMSO-d_6 as solvent and tetramethylsilane (TMS) as an internal standard at 500 MHz at room temperature. Electrospray ionization mass spectra (ESI–MS) were recorded on an LCQ system (Finnigan MAT, USA) using acetonitrile as the mobile phase. The spray voltage, tube lens offset, capillary voltage, and capillary temperature were set at 4.50 kV, 30.00 V, 23.00 V and 200 °C, respectively and the quoted *m/z* values are for the major peaks in the isotope distribution.

2.2. Synthesis of complexes

2.2.1. Preparation of ligand IPPH

A mixture of 1,10-phenanthroline-5,6-dione (0.315 g, 1.5 mmol), helicine (0.426 g, 1.5 mmol), NH_4Ac (2.31 g, 30 mnol) was dissolved in ethanol (20 mL), then the mixture was refluxed at 78 °C for 3 h, after cooling to room temperature, pale yellow precipitate was collected. The precipitate was washed three times with ice water, the yellow powder was obtained. Yield: 79%. Anal. Cacld for $C_{25}H_{22}N_4O_6$: C, 63.29, H, 4.67, N, 11.81%. Found: C, 63.53, H, 4.34, N, 11.98%. ESI-MS (CH_3OH): *m/z* = 473.20 ([M-1]).

2.2.2. Synthesis of complex $[Ir(ppy)_2(IPPH)]PF_6$ (*Ir1*)

A mixture of cis-$[Ir(ppy)_2Cl]_2$ (0.28 g, 0.25 mmol) [40] and IPPH (0.237 g, 0.5 mmol) was dissolved in 42 mL of dichloromethane and methanol (*v*/v, 2:1). The mixture was refluxed at 40 °C for 6 h under the protection of argon. Upon cooling, saturated aqueous NH_4PF_6 was added to the reaction solution with stirring at room temperature for 2 h to obtain yellow precipitate. The crude product was initially separated using silica gel column with dichloromethane-acetone (*v*/v, 1:3) as eluent, the yellow band was collected. The solvent was removed under reduced pressure and the yellow powder was obtained. Yield: 83%. ^{1}H NMR (Acetone-d_6, 500 MHz): δ 9.25 (dd, 2H, *J* = 1.0, *J* = 8.5 Hz), 8.48–8.45 (m, 1H), 8.37 (d, 2H, *J* = 5.0 Hz), 8.24 (d, 2H, *J* = 8.5 Hz), 8.07–8.02 (m, 2H), 7.93 (d, 2H, *J* = 8.0 Hz), 7.89 (t, 2H, *J* = 8.0 Hz), 7.73 (d, 2H, *J* = 6.0 Hz), 7.58–7.55 (m, 1H), 7.49–7.45 (m, 1H), 7.39–7.34 (m, 1H), 7.08 (t, 2H, *J* = 6.0 Hz), 7.00–6.96 (m, 4H), 6.46 (d, 2H, *J* = 7.5 Hz), 5.26 (d, 1H, *J* = 8.0 Hz), 4.77 (s, 1H), 4.56 (s, 1H), 4.07–3.99 (m, 2H), 3.95–3.81 (m, 3H), 3.77–3.68 (m, 2H), 3.59 (t, 1H, *J* = 8.0 Hz). ^{13}C NMR (Acetone-d_6, 125 MHz): 168.59, 156.72, 150.19, 145.02, 139.30, 132.74, 132.54, 131.11, 130.65, 130.52, 127.68, 127.58, 125.67, 124.72, 124.68, 124.23, 123.29, 120.58, 120.25, 119.65, 119.61, 104.73, 78.57, 77.39, 75.23, 71.55, 68.85, 62.36. HRMS (CH_3CN): $C_{47}H_{38}N_6O_6IrPF_6$: *m/z* = 975.2463 $[(M\text{-}PF_6)^+]$.

2.2.3. Synthesis of complex $[Ir(piq)_2(IPPH)]PF_6$ (*Ir2*)

The complex $[Ir(piq)_2(IPPH)]PF_6$ (**Ir2**) was synthesized in an identical method that described for **Ir1**, with cis-$[Ir(piq)_2Cl]_2$ [40] in place of cis-$[Ir(ppy)_2Cl]_2$. Yield: 72%. ^{1}H NMR (Acetone-d_6, 500 MHz): δ 9.24 (dd, 2H, *J* = 1.0, *J* = 8.5 Hz), 9.11 (d, 2H, *J* = 8.5 Hz), 8.47 (d, 3H, *J* = 8.0 Hz), 8.26–8.24 (m, 2H), 8.04–7.99 (m, 4H), 7.91 (t, 2H, *J* = 6.5 Hz), 7.86 (t, 2H, *J* = 7.0 Hz), 7.75 (t, 1H, *J* = 7.5 Hz), 7.69 (t, 1H, *J* = 8.0 Hz) 7.61 (d, 2H, *J* = 6.5 Hz), 7.58–7.52 (m, 1H), 7.40 (d, 2H, *J* = 6.5 Hz), 7.38–7.29 (m, 1H), 7.19 (t, 2H, *J* = 7.5 Hz), 6.96 (t, 2H, *J* = 7.5 Hz), 6.48 (d, 2H, *J* = 7.0 Hz), 5.26 (dd, 1H, *J* = 2.5, *J* = 8.0 Hz), 4.76 (s, 1H), 4.55 (s, 1H), 4.07–4.00 (m, 2H), 3.95–3.81 (m, 3H), 3.76–3.67 (m, 2H), 3.58 (t, 1H, *J* = 8.0 Hz). ^{13}C NMR (Acetone-d_6, 125 MHz): 169.59, 156.73, 146.57, 141.79, 137.89, 133.03, 132.70, 131.50, 131.32, 130.63, 129.84, 128.39, 127.49, 126.96, 124.71, 123.08, 122.64, 120.24, 119.65, 104.76, 78.59, 77.39, 75.19, 71.54, 68.84, 62.36. HRMS (CH_3CN): $C_{55}H_{42}N_6O_6IrPF_6$: *m/z* = 1075.2966 $[(M\text{-}PF_6)^+]$.

2.3. pK_a values determination

The pK_a values of the complexes were assayed by potentiometric titration method using a pH meter (Basic pH Meter PB-10, Sartorius) calibrated with standard buffers of pH 4.01, 6.86 and 9.18. The complexes were dissolved in a mixture of acetonitrile and water (*v*/v, 3:7). The pH value of the above mixture was adjusted to 2 using HCl solution (100 mM) under constant ionic strength (150 mM, KCl). Then KOH solution (60 mM) was added until the pH value reaches 12.

Table 1
IC_{50} values (μM) of the ligand and its complexes toward the selected cancer cells for 48 h.

Complexes	BEL-7402	A549	HCT116	B16	LO2
IPPH	> 100	79.6 ± 4.1	> 100	> 100	> 100
IPPH (light)	> 100	> 100	28.6 ± 3.8	> 100	> 100
Ir1	>100	>100	>100	>100	>100
Ir1(light)	30.8 ± 0.8	16.8 ± 2.1	18.0 ± 1.3	35.5 ± 3.5	>100
Ir2	>100	>100	>100	>100	>100
Ir2 (light)	5.0 ± 0.4	0.2 ± 0.05	0.8 ± 0.1	32.4 ± 0.9	26.1 ± 3.6
Cisplatin	15.4 ± 4.1	6.5 ± 0.5	15.6 ± 0.4	20.3 ± 1.0	18.7 ± 0.7

Data for cisplatin toward A549, BEL-7402 and LO2 from ref. [52], HCT116 from ref. [53].

2.4. Cell culture

A549, HCT116, B16 and normal LO2 were cultured in Dulbecco's Modified Eagle Medium (DMEM). BEL-7402 cells were cultured in the Roswell Park Memorial Institute (RPMI) 1640. The medium for the culture of cell lines was supplemented with 10% (*v*/v) fetal bovine serum (FBS, Gibco, USA) and 1% (v/v) the penicillin-streptomycin solution. All cells were cultured at 37 °C in a humidified atmosphere consisting of 5% CO_2 and 95% air.

2.5. Cytotoxicity assay in vitro

The cytotoxic activity of **Ir1** and **Ir2** in vitro against the selected cancer cell lines was assayed by 3-(4,5-dimethylthiazole-2-yl)-2,5-biphenyl tetrazolium bromide (MTT) method [41]. The cells were seeded in a 96-well microplate (Costar, Corning Corp, New York) at a density of 1.0×10^4 cells per well and further grown overnight at 37 °C in a 5% CO_2 incubator. Next, different concentration (0–100 μM) of the complexes dissolved in DMSO (final concentration of DMSO of 0.05%, *v*/v) were added to the wells. Light activation of complexes was performed with visible light and the cells were irradiated with a 65 w LED lamp (white light, 5.2 J cm^{-2}). The distance between the lamp and the 96-well plate was 20 cm and the temperature was maintained at room temperature for 40 min during the irradiation period. After incubation at 37 °C in 5% CO_2 for 48 h, replacing the medium in the wells with 90 μL of medium and 10 μL of MTT dye solution (5 mg/mL) and the incubation was allowed to continue for another 4 h. The formed formazan crystals were dissolved in 100 μL DMSO according to MTT Kit. Absorbance was measured at 490 nm by a Microplate Reader (Multiskan FC, Thermo Scientific, Shanghai, China). The obtained results were analyzed with the IBM SPSS Statistics (version 20.0) to obtain the mean IC_{50} values in the independent three experiments.

Note: In the following experiments, the location and cellular uptake were performed without irradiation, in the other cell experiments, the cells were treated with IC_{50} concentration of the complexes for 4 h, then the cells were irradiated with white light (65 w LED lamp, light dose of 5.2 J cm^{-2}, λ = 450–465 nm) for 40 min.

2.6. Cellular uptake

A549 cells (1×10^5 cells per well) were inoculated into 12-well plates and grown to 50% of the density. After adding 10.0 μM concentration of **Ir1** and **Ir2**, the cells were incubated at 37 °C and 5% CO_2 for 4 h. Then, removing the culture medium, the nuclei were stained with 4′,6-diamidino-2-phenylindole (DAPI) at 37 °C for 20 min. The cells were washed thrice with cold phosphate buffer solution (PBS) and imaged under the ImageXpress R Micro XLS System (MD company, USA).

2.7. Wound healing assay

A wound healing test was used to examine the effects on the migration of A549 cells. The cells were seeded in a 6-well plate (5.0×10^5 per well) and incubated for 24 h. The cells were wounded with a sterile pipette tip and washed three times with PBS to remove any residual cell fragments from the scratch. Then, A549 cells were cultured with a fresh medium containing 1% FBS. After the addition of the complexes, 40 min of irradiation to the cells and continued to incubate for 24 h. Finally, images were taken at 0 and 24 h under an inverted microscope (Olympus Co., Tokyo, Japan). The wound width was analyzed using Image J software to quantify the speed of wound healing.

2.8. Measurement of apoptosis by flow cytometry

Apoptosis was assessed using Annexin V- FITC apoptosis detection kit according to the manufacturer's instructions. A549 cells were exposed to the IC_{50} concentrations of **Ir1** and **Ir2** and incubated at 37 °C in 5% CO_2 for 24 h. The cells were irradiated for 40 min. Then the cells were collected and treated with trypsin-EDTA solution. Eventually, the cells were washed twice with cold PBS and stained with Annexin V-FITC

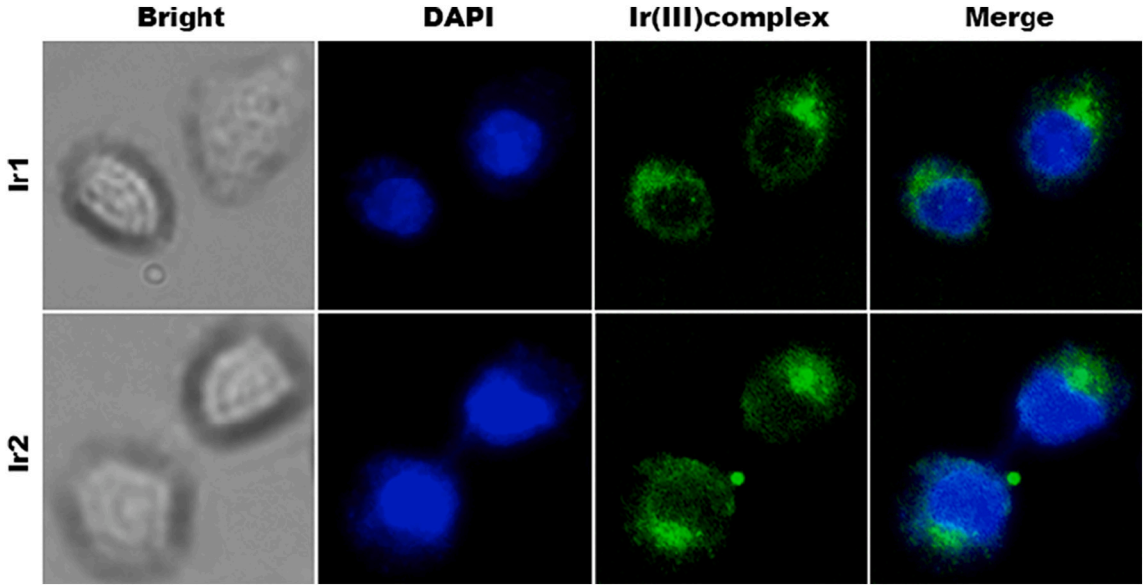

Fig. 1. The cellular uptake assay of A549 cells was incubated with **Ir1** (10 μM), **Ir2** (10 μM) for 4 h.

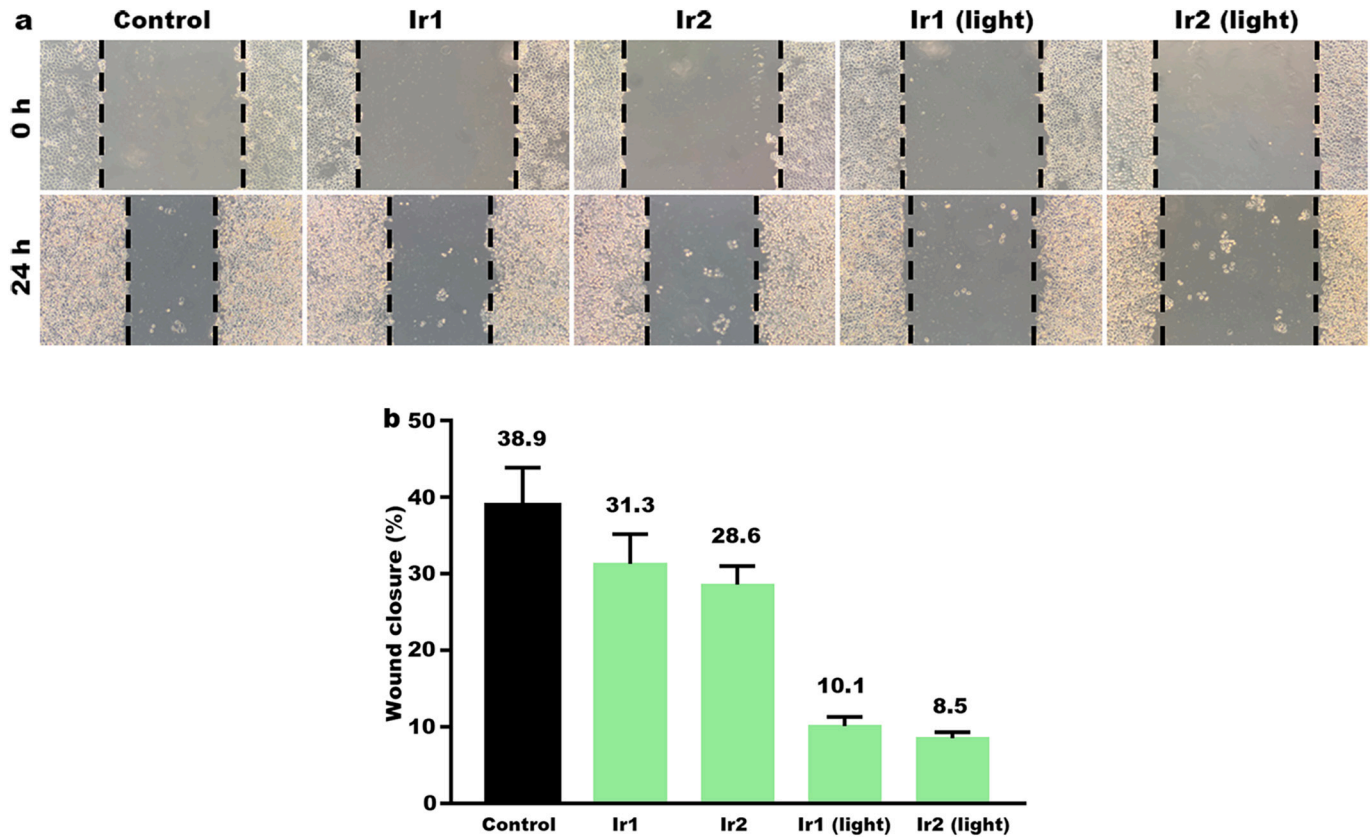

Fig. 2. (a) The wound healing studies after A549 cells were treated with IC_{50} concentration of **Ir1**, **Ir2** for 24 h upon irradiation. (b) The wound closure ratio values were analyzed with Image J.

(2 μL) and propidium iodide (PI, 2 μL) for 20 min in the dark. The apoptosis rates were immediately determined by flow cytometry (Beckman Instruments, NJ).

2.9. Cell cycle arrest determination

A549 cells were cultured in a 6-well plate (4×10^5 cells per well) overnight and incubated with IC_{50} concentration of **Ir1** and **Ir2**. After 4 h, the cells were irradiated for 40 min. Then the cells were harvested by trypsinization and centrifuged 5 min at 1000 *g*. The supernatant was carefully aspirated, washed with cold PBS and fixed with 75% ethanol at 4 °C overnight. According to guidance of the manufacturer's instructions, the cells were washed thrice with PBS and resuspended in 200 μL of assay buffer with 0.1% Triton X-100, 4 μL of PI (propidium iodide, 0.02 mg/mL) and 4 μL of RNase (ribonuclease, 0.2 mg/mL), and kept at room temperature for 30 min in the dark. The cells were analyzed by flow cytometry (Beckman Instruments, NJ).

2.10. Endoplasmic reticulum localization

The A549 cells were seeded in a 12-well plate at a density of 1.0×10^5 cells per well. After incubation for 24 h, the cells were treated with IC_{50} concentration of **Ir1** and **Ir2** for 4 h. The cells were washed twice with cold PBS and then incubated with ER Tracker Red (1 μM) at 37 °C for 20 min. After that, the cells were washed twice with cold PBS and observed under ImageXpress R Micro XLS System (MD company, USA).

2.11. Mitochondrial localization and membrane potential determination (MMP)

The A549 cells were incubated with IC_{50} concentration of **Ir1** and **Ir2** for 4 h and further co-incubated with MitoTracker ® Deep Red FM (1 μg/mL) at 37 °C for 0.5 h. Subsequently, the cells were rinsed with cold PBS and photographed under ImageXpress Micro XLS system as soon as possible. To investigate the effect of complexes on mitochondrial membrane potential (MMP), A549 cells were treated with the IC_{50} concentration of **Ir1** and **Ir2** for 24 h. Four hours after the addition of the complexes, the cells were irradiated for 40 min. The cells were stained with 5,5′-6,6′-tetrachloro-1,1′-3,3′-tetrethylbenzimidalylcarbocyanine iodide (JC-1) at 37 °C for 30 min after trypsin and collection. After centrifugation to remove the supernatant, the cell pellet was suspended in PBS. The ratio of red/green fluorescence intensity was measured by FACS Calibur flow cytometry (Beckman Instruments, NJ).

2.12. Determination of reactive oxygen species (ROS)

A549 cells were placed into a 12-well plate and incubated overnight. After discarding the medium, fresh DMEM containing IC_{50} concentration of **Ir1** and **Ir2** was added and incubated for 4 h at 37 °C in 5% CO_2, the cells were irradiated (white light) for 40 min. After 24 h, the cells were stained with 10 μM of 2′,7'-Dichlorodihydrofluorescein diacetate (DCHF-DA) in the dark. The cell nuclei were stained with 4′,6-Diamidino-2-phenylindole (DAPI) for 20 min and observed under the ImageXpress R Micro XLS System (MD company, USA).

2.13. Lipid peroxidation assay

The intracellular malondialdehyde (MDA) levels were measured using the thiobarbituric acid (Beyotime, Shanghai, China) method. Briefly, A549 cells were cultured in a 6-well plate (4×10^5 cells per well) for 24 h. After the density reached 90%, the IC_{50} concentration of the complexes were added to the cells for 4 h, then the cells were irradiated for 40 min, after 24 h, the cells were harvested by trypsinization, prepared in lysis buffer and centrifuged at 12,000 *g* for 15 min at 4 °C. The

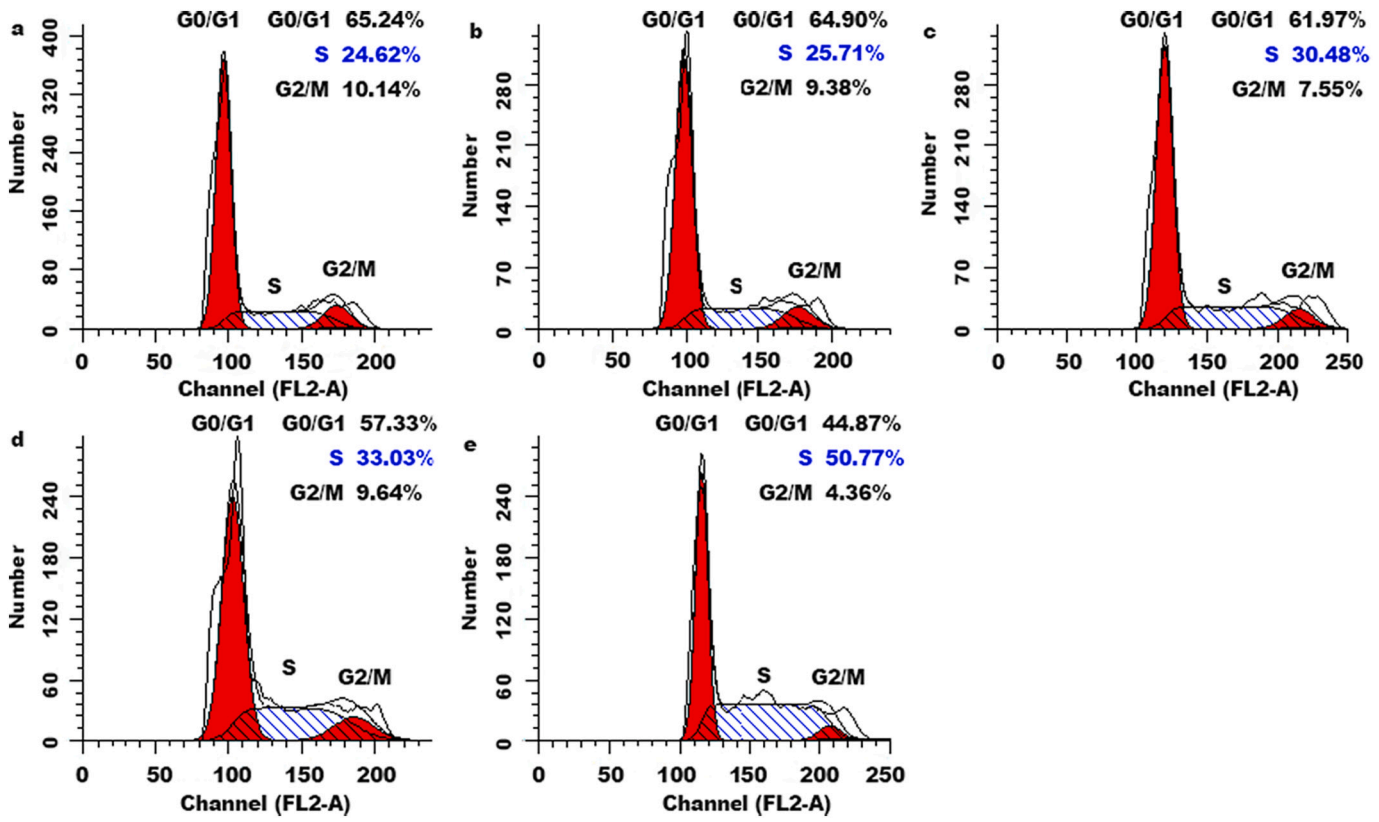

Fig. 3. Cell cycle distribution of A549 cells (a) were treated with IC_{50} concentration of **Ir1** (b) and **Ir2** (c) (without irradiation) or **Ir1** (d) and **Ir2** (e) (irradiation for 40 min).

supernatants were reacted with TBA (thiobarbituric acid) and the reaction products were measured spectrophotometrically at 530 nm. The concentration of MDA was calculated by a calibration curve using 1,1,3,3-tetrathoxypropane propane as a standard and expressed as μg/g protein.

2.14. Measurement of CRT, HSP70, HMGB1

A549 cells were seeded in a 12-well plate at the density of 1.0×10^5 cells/well and incubated overnight. Then, the cells were treated with IC_{50} concentration of **Ir1** and **Ir2** for 4 h, the cells were irradiated for 40 min. After 24 h, the cells were fixed with 75% alcohol, incubated with an immunostaining blocker for 1 h. Then the cells were incubated with rabbit antibodies (CRT, HSP70 and HMGB1) at 1:70 dilutions at 4 °C overnight. Next, the plate was washed with immunol staining wash buffer three times and incubated with FITC-labeled Goat Anti-Rabbit IgG in the dark for 1 h. After that, the cells were washed twice, then stained with DAPI for 20 min, and the images of CRT, HSP70 and HMGB 1 expression were obtained under the ImageXpress Micro XLS System (MD company, USA).

2.15. Immunofluorescence staining of γ-H2AX

Immunofluorescence staining for γ-H2AX was measured using the DNA damage assay kit by γ-H2AX immunofluorescence (Beyotime, Shanghai, China). A549 cells were treated with IC_{50} concentration of **Ir1** and **Ir2** for 4 h in a 12-well plate (1.0×10^5 cells/well), the cells were irradiated for 40 min. After 24 h, the cells were washed three times with cold PBS and blocked at 4 °C for 1 h using QuickBlock™ Blocking Buffer for Immunol Staining. Then the cells were incubated for 1 h at room temperature with an anti-γ-H2AX primary antibody (rabbit monoclonal; Beyotime, Shanghai, China; 1:200). A549 cells were washed with Immunol Staining Wash Buffer containing 0.5% Triton X-100 and incubated with a fluorescein isothiocyanate (FITC)-conjugated secondary antibody (Beyotime, Shanghai, China; 1:200) for 80 min at 4 °C. The nuclei were stained with 4,6-diamidino-2-phenylindole (DAPI) and images were acquired under Micro XLS System (MD company, USA).

2.16. Western blotting assay

A549 cells were seeded into a 6-well plate at a density of 2.0×10^6 cells per well for 24 h and treated with IC_{50} concentrations of the **Ir1** and **Ir2** for 4 h, the cells were irradiated for 40 min. After 24 h, the cells were washed three times with cold PBS and lysed in lysis buffer (phosphatase and protease inhibitor mixture) on ice and centrifuged at 12,000 rpm for 15 min at 4 °C. The protein content of the sample was detected using a BCA assay. Samples with equal protein concentrations were separated by 10 or 15% sodium dodecyl sulfate polyacrylamide gel electrophoresis (SDS-PAGE). Separated proteins were transferred from the gels to polyvinylidene difluoride (PVDF) membranes. The membranes were blocked with 5% skim milk in TBST (20 mM Tris–HCl, 150 mM NaCl, 0.2% Tween 20, pH 8.0) buffer for 1 h at room temperature and incubated with primary antibodies in diluent overnight at 4 °C. The polyvinylidene difluoride (PVDF) membranes were washed four times with TBST and incubated with secondary antibodies conjugated with horseradish peroxidase (1:5000 dilution) for 70 min. Finally, the membranes were washed three times with TBST and developed with BeyoECL Star solution, followed by imaging with FluorChem instrument (ProteinSimple, CA, USA). The protein expression level was analyzed using the Image J software.

2.17. Data analysis

The results were expressed as mean ± SD. Statistical significance was evaluated through a one-way analysis of variance. The $^*P$ values <0.05 was considered statistically significant.

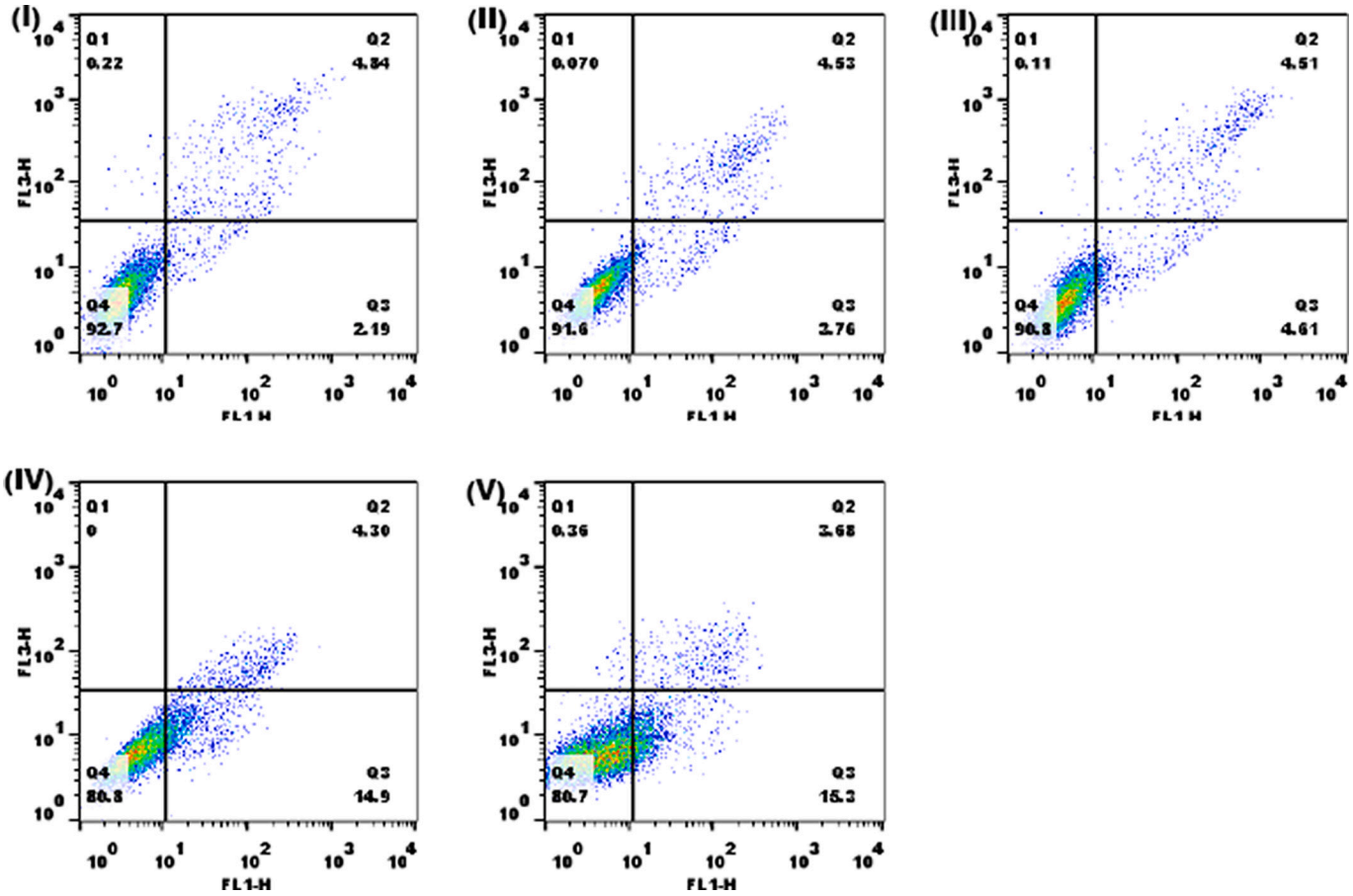

Fig. 4. Apoptosis assay of A549 cells (I) exposure to IC_{50} concentration of **Ir1** (II), **Ir2** (III) (without irradiation) or **Ir1** (IV) and **Ir2** (V) upon irradiation for 40 min.

3. Results and discussion

3.1. Synthesis and characterization

The ligand IPPH was prepared through condensation of 1,10-phenanthroline-5,6-dione with helicine in the ethanol. The complexes **Ir1** and **Ir2** were synthesized by the direct reaction with $[Ir(ppy)_2Cl_2]_2$ or $[Ir(piq)_2Cl_2]_2$ and IPPH in a mixture of dichloromethane and methanol under argon. The crude product was purified on a silica gel (100–200 mesh) column and dichloromethane–acetone (1:3, *v*/v) as eluent. The complexes were characterized by HRMS, ^{1}H NMR and ^{13}C NMR. In the spectra of HRMS, the signal of $[M\text{-}PF_6]^+$ was observed, the determined molecular weights are consistent with the expected values. The purity of the complexes was detected using methanol and water ($V_{methanol}$:V_{water} = 97:3 for **Ir1**, 95:5 for **Ir2**) as mobile phase by HPLC. As shown in Fig. S1 (supporting information), during the period of 30 min, only a peak for **Ir1** and **Ir2** was discovered, indicating that the complexes are pure.

The UV–Vis spectra of 20.0 μM **Ir1** and **Ir2** in ethanol were shown in Fig. S2a (supporting information), the maximum absorbance of **Ir1** and **Ir2** appeared at 277 (ε = 57,595), 289 (ε = 67,630) nm, respectively. The complexes can luminescence in ethanol at room temperature, with a maximum for **Ir1** and **Ir2** (Fig. S2b, supporting information) appearing at 559 nm (λ_{ex} = 275 nm) and 589 nm (λ_{ex} = 290 nm), respectively. The luminescence of the complexes in PBS solution was also detected, the complexes emit weak green fluorescence (Fig. S2c, supporting information).

The luminescence quantum yield (Φ) of the complexes was determined under argon according to the literature [42] using $[Ru(bpy)_3]^{2+}$ (Φ = 0.04, methanol) as a refence, the complexes (10 μM) were dissolved in methanol and diluted with water. The Φ values were calculated according to the following equation:

$$\Phi_c = \Phi_r \times \left(I_c A_r n_s^2 / I_r A_c n_r^2\right)$$

Where *I* is integrated emission intensity, *A* is absorbance intensity, *n* is refractive index of solvent. The subscript *r* stands for reference, *c* stands for the complexes.

The luminescence quantum yields for **Ir1** and **Ir2** were determined to be 0.13 and 0.05.

The stability of the complexes in PBS solution at room temperature was detected at 0 and 24 h, as shown in Fig. S3 (supporting information), no change in the shape of the peaks was observed, indicating that the complexes are stable in PBS solution.

3.2. pK_a values determination

The dissociation constant (pK_a) of the complexes has a considerable influence on the physicochemical and pharmacokinetic properties and can be used to determine whether it can cross the blood-brain barrier [43]. Compounds with minimally one charge with a $pK_a > 4$ for acids and correspondingly a $pK_a < 10$ for bases can cross the cell membrane by passive diffusion [44]. The pH values for **Ir1** and **Ir2** are 6.61 and 6.29, respectively. The pK_a values were obtained by a graph of pH versus volume of KOH. As shown in Fig. S4 (supporting information), the pK_a values are 7.13 for **Ir1**, 7.02 for **Ir2**, indicating that the complexes can cross the cell membrane to enter to the cells.

3.3. Irradiation increases the cytotoxicity

The cytotoxicity of IPPH, **Ir1** and **Ir2** toward BEL-7402, A549, HCT-

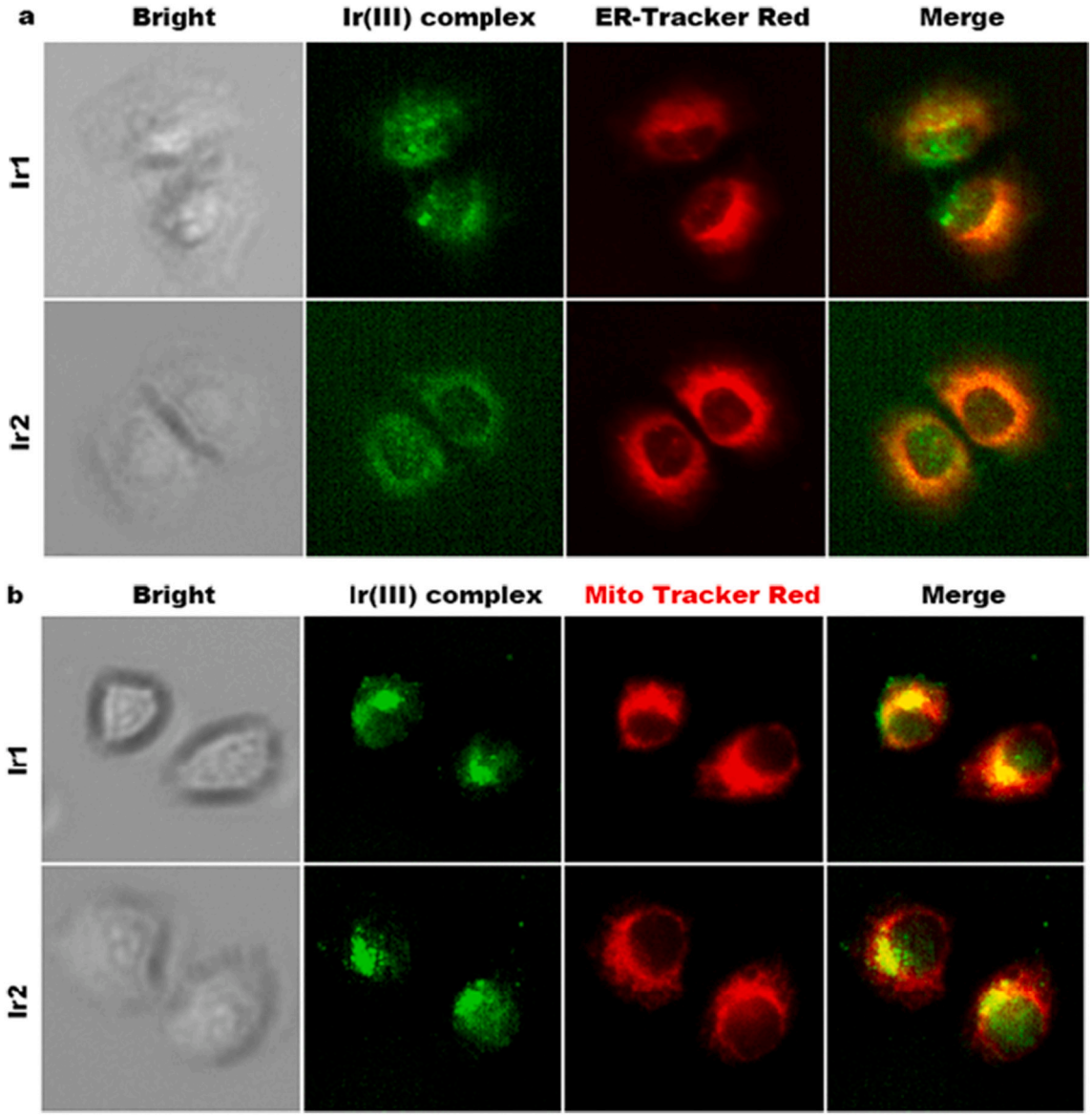

Fig. 5. Location assay (a) endoplasmic reticulum and (b) mitochondria of A549 cells incubated with IC_{50} concentration of **Ir1** and **Ir2** for 4 h and stained with ER-Tracker Red or Mito-Tracker Red. (For interpretation of the references to colour in this figure legend, the reader is referred to the web version of this article.)

116, B16 cancer cells and normal LO2 was determined by MTT assay. The obtained IC_{50} values are listed in Table 1. As expected, IPPH shows no or low cytotoxic activity. Unexpectedly, complexes **Ir1** and **Ir2** show weakly cytotoxic activity against BEL-7402, A549, HCT-116, B16 cancer cells and normal LO2 cells ($IC_{50} > 100$ μM). To enhance anticancer activity of the complexes, the cells were treated with different concentration of the complexes for 4 h, then the cells were irradiated with white light (65 w LED lamp, light dose of 5.2 J cm^{-2}, λ = 450–465 nm) for 40 min, the complexes showed remarkable activity against all the cancer cells. In particular, **Ir2** exhibits very high ability to kill A549 and HCT116 cells with a low IC_{50} value of 0.2 ± 0.05 and 0.8 ± 0.1 μM. Comparing the IC_{50} values, **Ir2** shows higher cytotoxic activity than **Ir1** and cisplatin under the identical conditions. Hence, irradiation can increase the cytotoxic activity of the complexes toward cancer cells. Gupta et al. synthesized a Ir(III) dipyrrinato complex with sugar moiety (WSIr7), the IC_{50} values of the complex against A549 cells are 84.3 ± 1.9 and 17.8 ± 0.5 μM in the dark and in the presence of light, respectively. The phototoxicity index (PI) shows that the photosensitizer (WSIr7) is about 4 times more active under light than under the dark conditions [45]. While **Ir2** has no cytotoxic activity in the dark ($IC_{50} > 100$ μM), in the presence of white light, **Ir2** exhibits very high anticancer effect on A549 cells with a very low IC_{50} value ($IC_{50} = 0.2 \pm 0.05$ μM). Therefore, **Ir2** exhibits higher photosensitizer efficacy toward A549 cells than WSIr7, $[Ir(ppy)_2(ipbc)](PF_6)$ (ipbc = 4′-(1H-imidazo[4,5-f][1,10]phenanthrolin-2-yl)-(1,10-biphenyl)-4-carbaladehyde, IC_{50} = 48.5 ± 3.8 μM, light) [46] and $[Ir(ppy)_2(FBPIP)][(PF_6)$ (FBPIP = 2-(4-formyl)benzeno[4,5-f][1,10]phenanthroline, IC_{50} = 22.9 ± 1.2 μM) [47]. Similar results were observed for the cytotoxic activity of other families of iridium(III) complexes [31,32]. In general, upon irradiation, the complexes can increase intracellular ROS (e.g. superoxide, hydroxyl radicals or peroxides) and $^1O_2$. Both ROS and $^1O_2$ rapidly interact with adjacent biomolecules disrupting normal cell functions that finally drives to cell death [48,49]. According to the literature [50,51], we infer iridium(III) complexes **Ir1** and **Ir2** can effectively sensitize ground-state oxygen ($^3O_2$) to produce cytotoxic singlet oxygen ($^1O_2$), making them highly effective photosensitizers for use in photodynamic therapy (PDT). Notably, **Ir1** and **Ir2** displayed strong PDT efficacy under irradiation and **Ir2** can be used as photosensitizer for the treatment of cancer. Based on these results, A549 cells were chosen for the undergoing experiments.

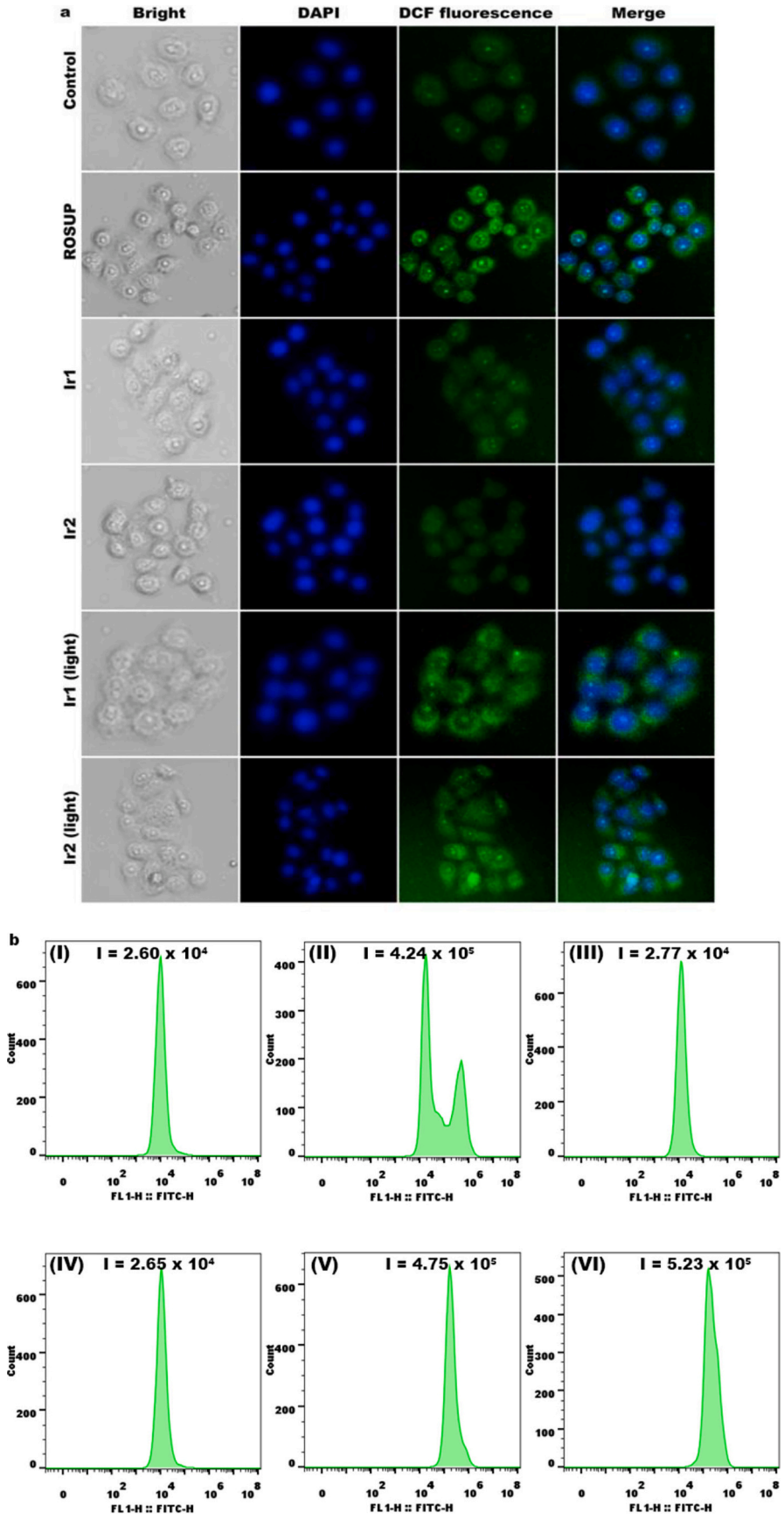

Fig. 6. (a) Intracellular ROS assay of A549 cells exposure to ROSUP, IC_{50} concentration of **Ir1** or **Ir2** in the absence or presence of irradiation. (b) Assay of DCF fluorescence intensity after 24 h exposure of A549 cells (I) to ROSUP (II), IC_{50} concentration of **Ir1** (III, V) or **Ir2** (IV, VI) in the absence or presence of irradiation.

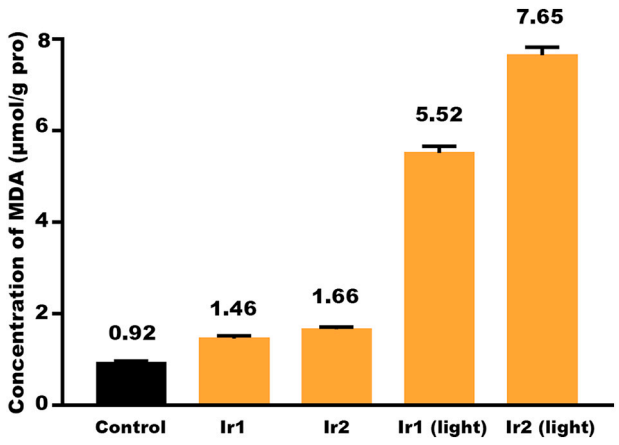

Fig. 7. The determination of the concentration of MDA in A549 treated with IC_{50} concentration of **Ir1** and **Ir2** upon irradiation or not for 40 min.

3.4. Analysis of the uptake of complexes

The cellular uptake was monitored under the ImageXpress High Content Screening System. A549 cells were treated with **Ir1** (10 μM) and **Ir2** (10 μM) for 4 h and stained by DAPI (λ_{ex} = 340 nm, λ_{em} = 488 nm), as the fluorescence probe. As shown in Fig. 1, **Ir1** and **Ir2** emit green fluorescence due to autofluorescence properties, and the cell nuclei were stained blue. The merge of the green and blue fluorescence indicates that the complexes successfully crossed the cell membrane and entered the cell and mainly distribute in the cytoplasm and few amount of the complexes distribute in the cell nuclei.

3.5. Wound healing assays

The tendency of tumor cells to metastasize and spread is a major cause of cancer treatment failure [54]. A wound healing assay is a standard technique in vitro to evaluate cell migration capacity [55]. As shown in Fig. 2a and b, compared with the control group, **Ir1** and **Ir2** could attenuate the healing of wounded cell monolayers to a certain extent, but still could not stop the tendency of A549 cell migration. However, after irradiation, **Ir1 (light)** and **Ir2 (light)** can effectively inhibit the cell migration, and the width of the wound's edge was almost unchanged. Wound area analysis showed that a significant reduction in the percent of wound closure was observed in A549 cells exposed to photoactivated **Ir1** and **Ir2** compared to control cells. While **Ir1** and **Ir2** show weak ability to prevent the cell migration without irradiation. Therefore, the above results indicated that the complexes effectively hindered the migration of A549 cells upon irridiation and follow the order of **Ir2 (light) > Ir1 (light) > Ir2 > Ir1**.

3.6. Cell cycle arrest analysis

To determine whether the complexes regulate the cell cycle, A549 cells were treated with IC_{50} concentration of **Ir1** and **Ir2** for 24 h stained with propidium iodide (PI), and cell cycle distribution was analyzed by flow cytometry. As shown in Fig. 3, in the control, the percentage of A549 cells in the S phase was 24.62%. Treatment of A549 cells with IC_{50} concentration of **Ir1** and **Ir2** for 24 h, the percentages in the cells at S phase are 25.71% and 30.48%, respectively. The slight changes in inhibition of S phase were observed for the complexes without irradiation. However, A549 cells exposure to IC_{50} concentration of **Ir1** and **Ir2** for 4 h, the cells were irradiated for 40 min, the percentages in the cells at S phase are 33.03% and 50.77%, an increase of 8.41% for **Ir1** and 26.15% for **Ir2** at the S phase compared with that in the control was found, accompanied by a corresponding decrease in the G0/G1 phase. The results further demonstrate that photoactivation of complexes can greatly increase the anticancer efficacy.

3.7. Analysis of inducing apoptosis

Apoptosis, the programmed cell death, is finely regulated at the gene levels resulting in the efficient removal of damaged cells [56]. Therefore, we further investigated the effect of the complexes on apoptosis in the presence or absence of irradiation. As shown in Fig. 4, in the control (I), the percentage of early apoptosis was 2.19%. without irradiation, **Ir1** (II) and **Ir2** (III) cause a weak apoptotic effect. After irradiation for 40 min, the early apoptotic rate reached 14.9% and 15.3% after treatment with IC_{50} concentration of **Ir1** (IV) and **Ir2** (V), the apoptotic percentage increases by 12.71% and 13.11% for **Ir1** and **Ir2**. This is consistent with the cell cytotoxic activity. These results reveal that the complexes can effectively induce apoptosis upon irradiation, and they may become promising PDT agents for the treatment of cancer.

3.8. Subcellular localization of the complexes

The endoplasmic reticulum (ER) is a specialized organelle that regulates protein homeostasis that orchestrates and monitors the synthesis, folding, assembly, trafficking and degradation of all proteins destined [57]. Homeostasis imbalance in ER results in ER stress which further induces apoptosis [58]. Most of the iridium(III) complexes containing N-based ligands, such as polypyridyl, N-heterocyclic carbene (NHC), phenanthroline, can accumulate in the ER membrane and mitochondria [30,59]. The location of the complexes at the endoplasmic reticulum and mitochondria after a 4 h exposure of A549 cells to IC_{50} concentration of **Ir1** and **Ir2** was further investigated under the ImageXpress Micro XLS System. As displayed in Fig. 5a, the green fluorescence of the complexes significantly overlaps with the red fluorescence of ER-Tracker Red (λ_{ex} = 587 nm, λ_{em} = 615 nm), suggesting that the complexes localized at the endoplasmic reticulum. The Pearson's colocalization coefficients (PCC) were calculated by analyzing the red and green fluorescence intensity (Image pro plus 6.0 software) in 50 cells according to literature [60]. The PCC values are 0.94 for **1** and 0.95 for **2**. To explore whether the complexes located at the mitochondria, A549 were treated with IC_{50} concentration of **Ir1** and **Ir2** for 4 h, the mitochondria were stained red with Mito-Tracker Red (λ_{ex} = 579 nm, λ_{em} = 599 nm). The complexes emit weak green fluorescence, the merge of the red and green fluorescence indicates that the complexes were localized at the mitochondria (Fig. 5b). The PCC values are 0.98 for **1** and 0.94 for **2**. The Pearson's colocalization coefficients for endoplasmic reticulum and mitochondria indicate an existence of positive correlation. Hence, according to the PCC values, we consider that the complexes accumulate both in the endoplasmic reticulum and mitochondria.

3.9. Cellular reactive oxidative species (ROS) production

In PDT, photosensitizers and tumor cells were exposed to transformation and endogenous molecular oxygen was converted to ROS ($^{\bullet}OH$, $O_2^{\bullet-}$, and $^1O_2$) [61,62]. The elevated cellular ROS levels activate various signaling pathways, causing mitochondrial injury and oxidative stress, which in turn induces apoptosis [63,64]. The distribution of the complexes in the mitochondria and the high phototoxicity induce cellular apoptosis promoted us to study intracellular ROS generation. The generation of reactive oxygen species (ROS) in A549 cells was measured using 2′,7′-dichlorodihydrofluorescein diacetate (DCHF-DA, λ_{ex} = 488 nm, λ_{em} = 525 nm) as fluorescence probe. DCHF-DA penetrates into the cell membrane to enter the cells and is hydrolyzed by intracellular esterase and converted into 2′,7′-dichlorodihydrofluorescein DCFH (non-fluorescent), which is rapidly oxidized by ROS into 2′,7′-dichlorofluorescein (DCF). The fluorescence of DCF and the levels of intracellular reactive oxygen species were positively correlated. As shown in Fig. 6a, when A549 cells were treated with IC_{50} concentration of the complexes **Ir1** and **Ir2** for 24 h, no obvious change of the

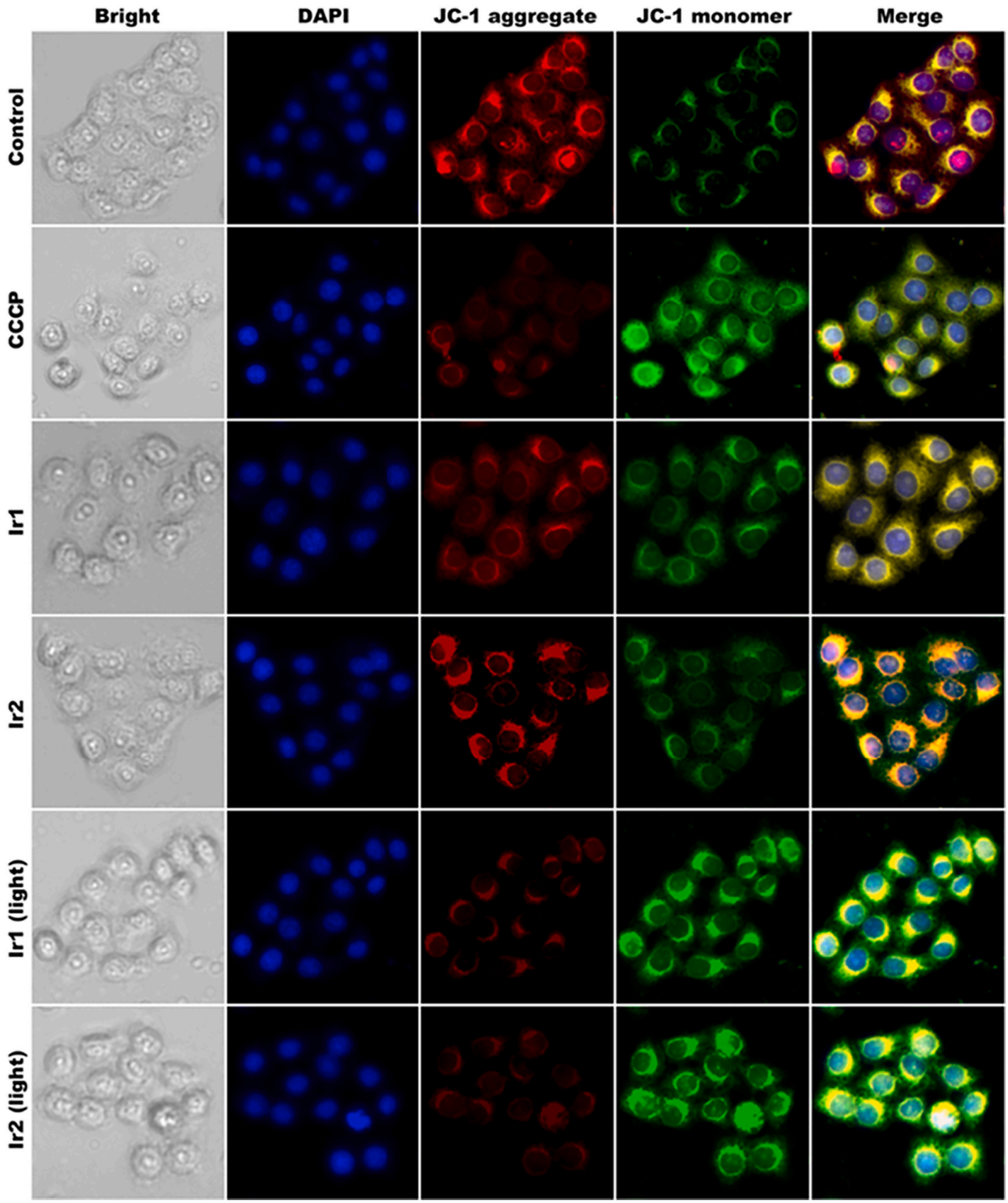

Fig. 8. Assay of mitochondrial membrane potential after A549 cells were exposed to CCCP (positive control) and IC_{50} concentration of **Ir1** and **Ir2** in the absence or presence of irradiation.

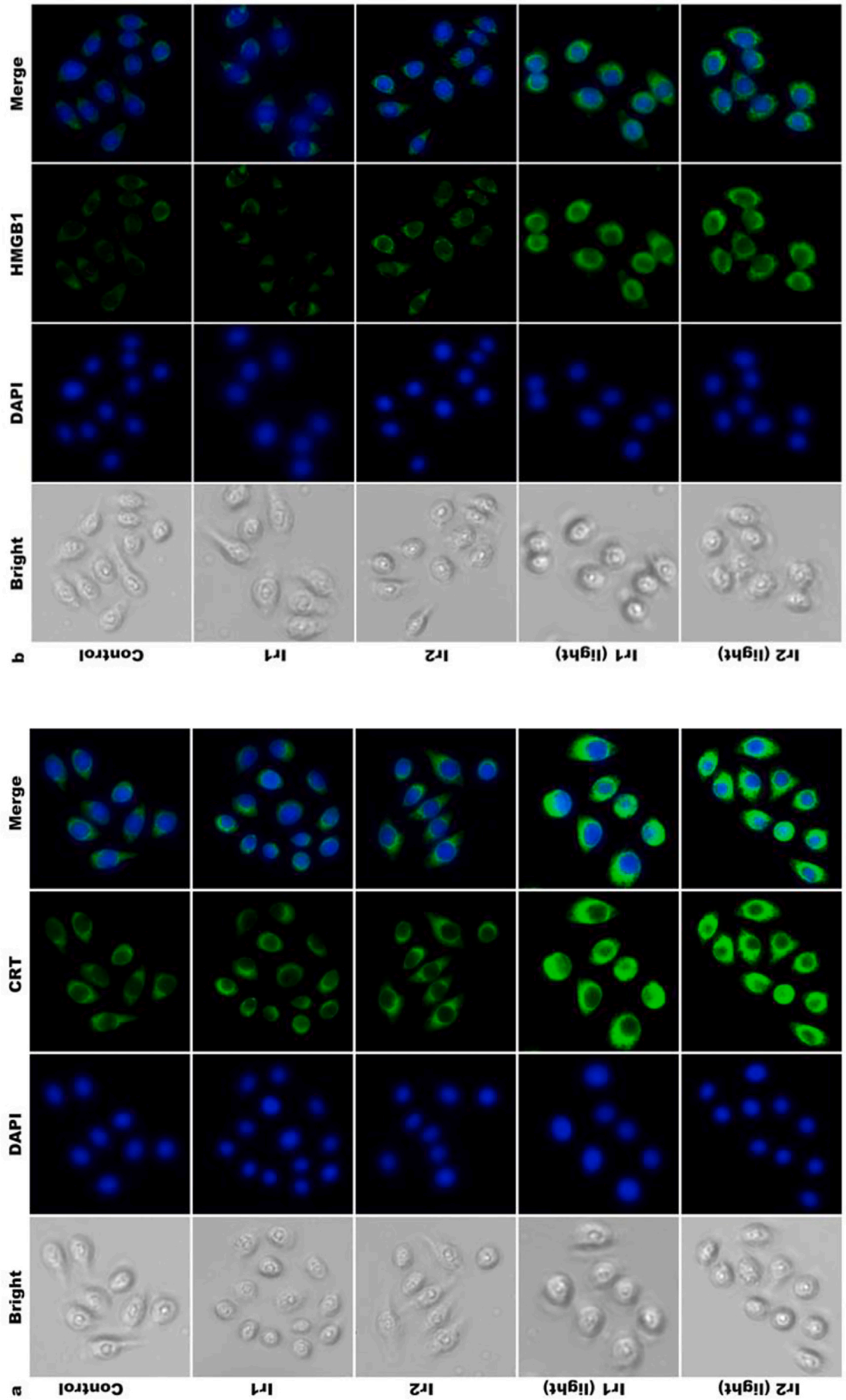

Fig. 9. Images of CRT (a), HMGB1 (b) and HSP70 (c) levels after A549 cells incubated with IC_{50} concentration of **Ir1** and **Ir2** for 24 h upon irradiation or not.

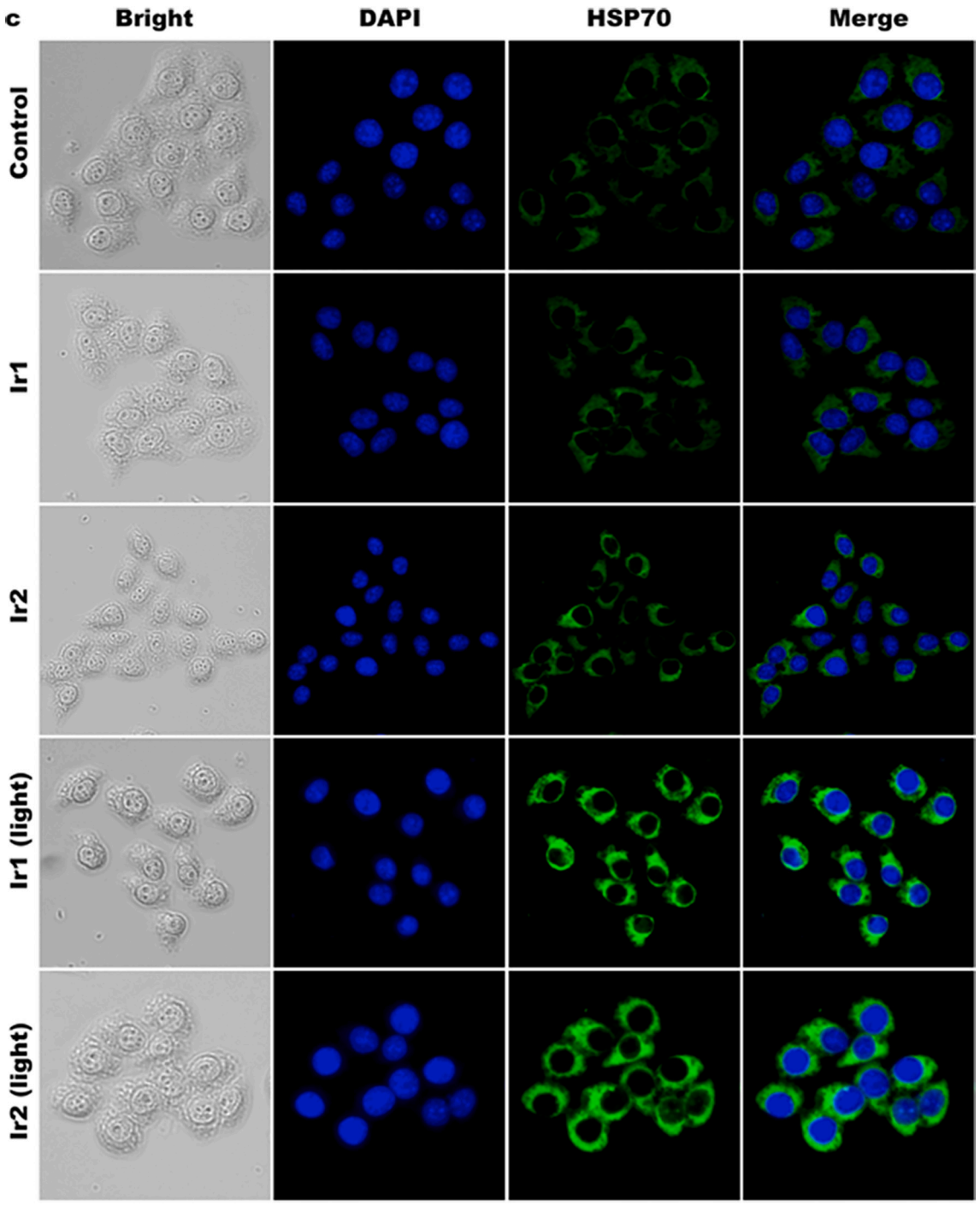

Fig. 9. (*continued*).

green fluorescence of intracellular DCF was observed compared with that in the control. However, under the irradiation of white light, the green fluorescence of A549 cells treated with ROSUP (positive control) and IC_{50} concentration of **Ir1** and **Ir2** was significantly enhanced, indicating that the complexes can increase intracellular ROS levels upon irradiation.

To quantitatively compare the efficacy of **Ir1** and **Ir2** on intracellular ROS levels, DCF green fluorescence intensity was determined by flow cytometry. As illustrated in Fig. 6b, in the control (I), the fluorescence intensity of DCF was 2.6×10^4. After A549 cells were exposed to ROSUP (II) and IC_{50} concentration of **Ir1** (III) and **Ir2** (IV), the green fluorescence intensity increases by 16.3, 1.07 and 1.02 times for ROSUP, **Ir1** and **Ir2**. However, upon irradiation, DCF fluorescence intensity increases by 18.3 and 20.1 times for **Ir1** (V) and **Ir2** (VI) compared with the control. Consequently, under irradiation, the complexes can greatly increase the intracellular ROS levels.

3.10. Detection lipid peroxidation levels

The excessive intracellular accumulation of reactive oxygen species contributes to lipid peroxidative damage promoting ferroptosis which is a form of regulated cell death [65,66]. To investigate the effect of the complexes on lipid peroxidation, the amount of lipid peroxidation product malondialdehyde (MDA) was measured in A549 cells. As

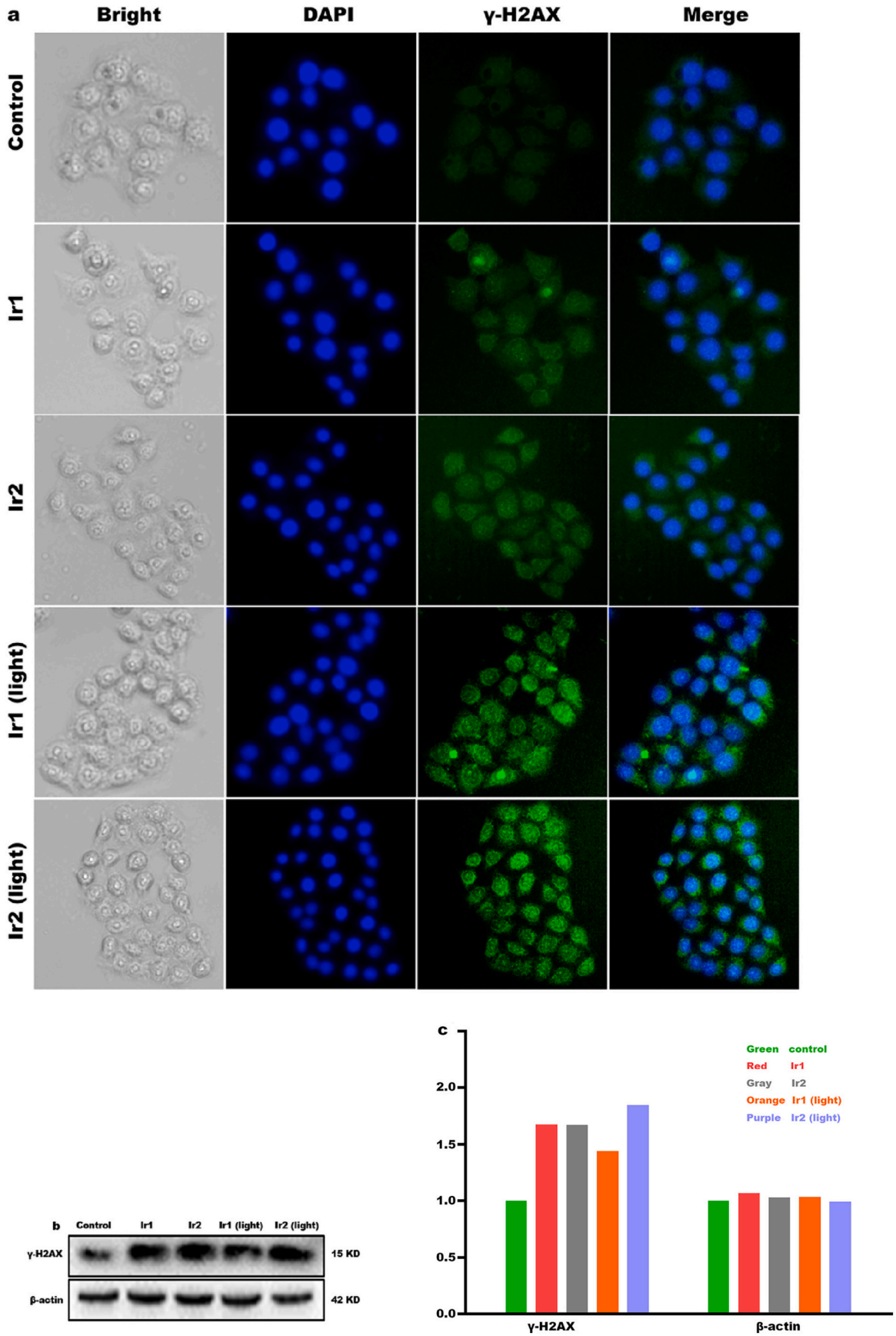

Fig. 10. (a) Immunofluorescence analysis of phosphorylated γ-H2AX induced by IC_{50} concentration of **Ir1** and **Ir2** in the absence or presence of white light photoirradiation. (b) Western blot analysis of γ-H2A after an exposure of A549 cells to IC_{50} concentration of **Ir1**, **Ir2** in the absence or presence of white light photoirradiation (450–465 nm, light dose = 5.2 J cm^{-2}). (c) The gray values of γ-H2AX protein.

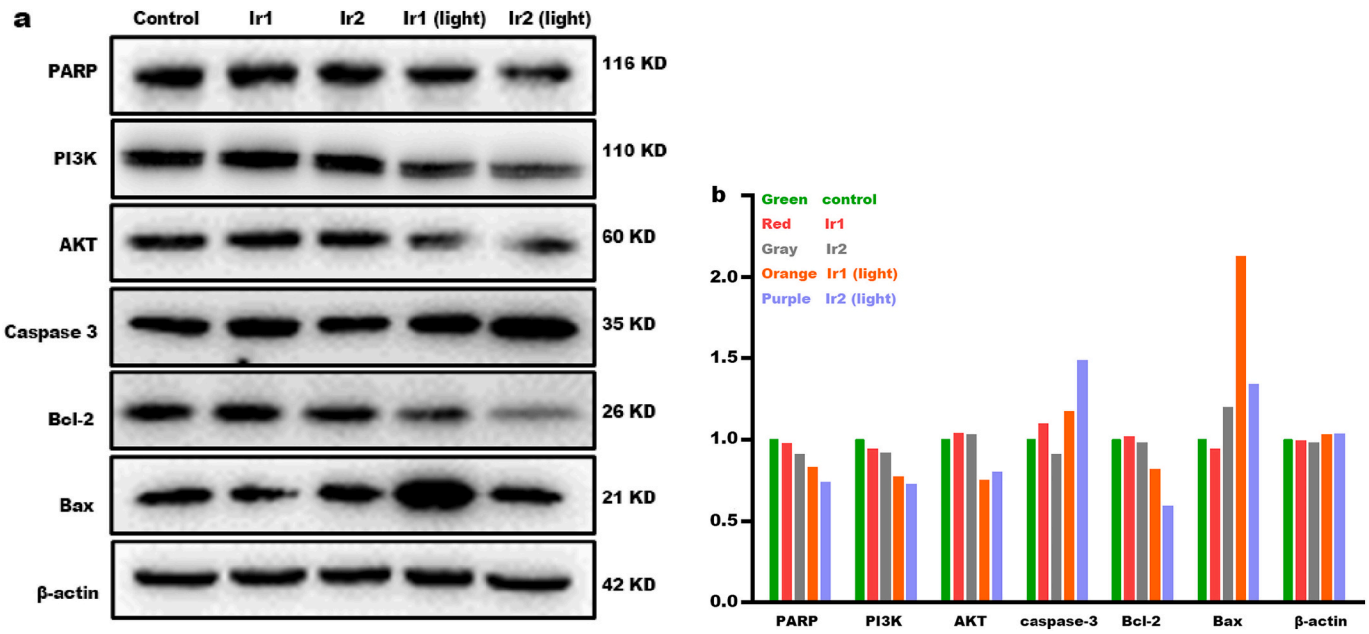

Fig. 11. (a) Western blot analysis of PARP, PI3K, AKT, caspase 3, Bcl-2 and Bax after an exposure of A549 cells to IC_{50} concentration of **Ir1**, **Ir2** in the absence or presence of irradiation (white light, 450–465 nm, light dose = 5.2 J cm^{-2}). (b) The quantitative values of the expression of PARP, PI3K, AKT, caspase 3, Bcl-2, Bax, β-actin was used as the internal control.

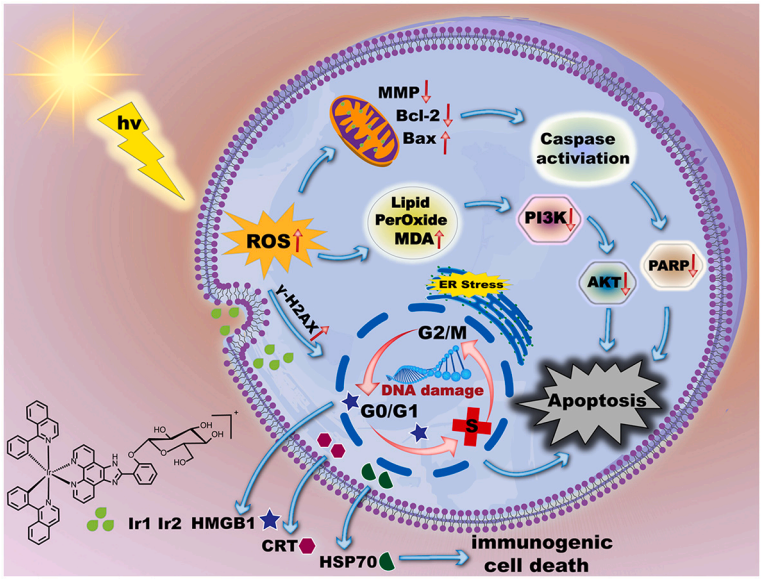

Fig. 12. The molecular mechanism of the complexes inducing apoptosis in A549 cells.

displayed in Fig. 7, compared with the control group, after an exposure of 24 h of A549 cells to IC_{50} concentration of **Ir1** and **Ir2**, a slight increase in the content of malondialdehyde (MDA) was discovered. However, A549 cells were treated with IC_{50} concentration of **Ir1** and **Ir2** upon irradiation for 40 min, the content of MDA increases by 6.00 times for **Ir1** and 8.32 times for **Ir2** compared with that in the control. These data demonstrated that the complexes can induce oxidant stress to promote ferroptosis of A549 cells upon irradiation.

3.11. Mitochondrial membrane potential assay

Mitochondrial membrane potential (MMP) is an indicator of mitochondrial activity and the oxidative stress caused by the accumulation of ROS in cells changes mitochondrial membrane permeability and triggers a decrease in mitochondrial membrane potential, which results in apoptosis [67–69]. The effect of the complexes on the mitochondrial membrane potential ($\Delta\Psi_m$) in A549 cells was investigated using dye 5,5′,6,6′-tetrachloro-1,1′,3,3′-tetraethylbenzimidazolylcarbocyanine iodide (JC-1, green, λ_{ex} = 514 nm, λ_{em} = 529 nm, red, λ_{ex} = 585 nm, λ_{em} = 590 nm) as fluorescence probe. JC-1 dye forms aggregates with red fluorescence at the high mitochondrial membrane potential. Conversely, the green fluorescence of the dye forms monomers corresponds to low mitochondrial membrane potential. A549 cells were treated with IC_{50} concentration of complexes **Ir1** and **Ir2** for 4 h and irradiated with white light (5.2 J cm^{-2}) for 40 min. After 24 h, the cells were stained with JC-1. See from Fig. 8, in the control, JC-1 dye exhibited bright red fluorescence and weak green fluorescence. Treatment of A549 cells with carbonylcyanide-*m*-chlorophenylhydrazone (CCCP, positive control)

and IC_{50} concentration of in the absence or presence of irradiation, the red fluorescence intensity decreases and the green fluorescence intensity increases compared with that in the control. The change from red to green fluorescence suggests that the complexes can cause a reduction of mitochondrial membrane potential.

3.12. Photoactivation of the complexes induces immunogenic cell death (ICD)

Upon irradiation, photosensitizers acting on the endoplasmic reticulum (ER) can cause robust ROS-based ER stress, thus inducing strong immunogenic cell death (ICD) characterized by inducing various damage associated molecular patterns (DAMPs) exposure [70]. ICD is characterized by translocation of calreticulin (CRT) from ER to the cell surface, secretion of heat shock protein 70 kDa (HSP70), migration of high mobility group box 1 (HMGB1) from the nuclei to the cytoplasm [71–73]. As shown in Fig. 9, A549 cells were treated with IC_{50} concentration of **Ir1** and **Ir2** for 24 h, in the absence of irradiation, no obvious change in the green fluorescence was discovered. However, upon irradiation for 40 min, the green fluorescence intensity enhances compared with that in the control. The degree of immunogenic cell death was reflected by the green fluorescence intensity of the antibody (containing fluorescein isothiocyanate (FITC, $\lambda_{ex} = 488$ nm, $\lambda_{em} = 518$ nm)) labeled CRT (a), HMGB1 (b) and HSP70 (c) proteins. These results showed that the complexes can induce immunogenic cell death upon irradiation.

3.13. γ-H2AX fluorescence intensity analysis

γ-H2AX is converted from phosphorylation of the Ser-139 residue of the histone variant H2AX, a recognized biomarker for the double-strand DNA breaks [74,75]. To quantitatively evaluate DNA damage, A549 cells were treated with IC_{50} concentration of **Ir1**, **Ir2** in the absence or presence of white light (λ = 450–465 nm, light dose = 5.2 J cm^{-2}, 40 min) for 24 h, and the expression level of γ-H_2AX (fluorescence dye FITC, $\lambda_{ex} = 488$ nm, $\lambda_{em} = 518$ nm) was evaluated by immunofluorescence staining. Fig. 10a illustrated that the control group showed a weak green fluorescence, IC_{50} concentration of **Ir1** and **Ir2** (without irradiation) showed relatively strong green fluorescence compared with the control. While in the A549 cells treated with IC_{50} concentration of **Ir1** and **Ir2** upon irradiation, bright green fluorescence was observed, indicating that the complexes can increase the content of γ-H2AX. In addition, the expression of γ-H2AX protein was investigated by western blot analysis. As shown in Fig. 10b and c, the expression of γ-H2AX protein in A549 cells was increased after treatment with the complexes compared with control, these data further confirm that **Ir1** and **Ir2** significantly cause DNA damage.

3.14. Expression of Bcl-2 family protein

To verify the effect of white light-activated complexes on the induction of apoptosis, the expression of B-cell lymphoma-2 (Bcl-2) family proteins was investigated by Western blot. The caspase family plays a key role in apoptosis, caspase 3 (cysteinyl aspartate specific proteinase-3) is activated to cleave the PARP in the early stages of apoptosis [74–77]. See from Fig. 11a and b, A549 cells were treated with IC_{50} concentration of **Ir1** and **Ir2** upon irradiation, compared to control, the expression levels of caspase 3, and the pro-apoptotic protein Bax (Bcl-2 associated x protein) were increased while the anti-apoptosis protein Bcl-2 and PARP (poly ADP-ribose polymerase) were reduced. The PI3K (phosphatidylinositol 3-kinase)/AKT (protein kinase B) signaling pathway regulates a variety of biological processes such as cell cycle, proliferation, apoptosis and is frequently aberrantly activated in human cancers [78–80]. Upon irradiation, **Ir1** (**light**) and **Ir2** (**light**) down-regulate the expression of PI3K and AKT compared with that in the control. Without irradiation, **Ir1** and **Ir2** show weak efficacy on the expression of caspase 3, PARP, Bax, Bcl-2, PI3K and AKT. Therefore, we inferred that the complexes strongly trigger apoptosis upon irradiation by regulating Bcl-2 family proteins and inhibiting the PI3K/AKT pathway.

4. Conclusions

In this article, two new complexes $[Ir(ppy)_2(IPPH)](PF_6)$ (**Ir1**) and $[Ir(piq)_2(IPPH)](PF_6)$ (**Ir2**) were synthesized and characterized by ESI-MS, UV, ^1H NMR and ^{13}C NMR. The MTT experimental results show that complexes **Ir1** and **Ir2** show weakly cytotoxic on the tested tumor cells. However, upon irradiation with white light for 40 min, the complexes exhibit significant phototoxicity, especially toward the A549 cell line with an IC_{50} value of 0.2 ± 0.05 μM for **Ir2**. Further studies have shown that the complexes localize at the endoplasmic reticulum (ER) and generate ER-stress induces immunogenic cell death, act on the mitochondria and increased the intracellular ROS, reduced the mitochondrial membrane potential. In addition, the western blotting showed that the complexes increased Bax/Bcl-2 ratio, caspase 3 and decreased PARP (poly ADP-ribose polymerase), PI3K (phosphoinositide-3 kinase) and AKT (protein kinase B). Meanwhile, the complexes caused DNA damage (upregulation of γ-H_2AX protein expression) and induce cell cycle arrest at S phase. In conclusion, this study demonstrates that photoactivatable iridium(III) complexes induce cell death in A549 through ROS-mediated endoplasmic reticulum stress-mitochondrial pathway, DNA damage pathway and ICD (Fig. 12). This work is helpful for design and synthesis new iridium(III) complexes as potent endoplasmic reticulum and mitochondria-targeted photodynamic therapy (PDT) candidates for cancer treatment.

Declaration of Competing Interest

Authors declare no competing interest exists.

Data availability

Data will be made available on request.

Acknowledgements

This work was supported by the National Natural Science Foundation of China (No 21877018) and the Natural Science foundation of Guangdong Province (No. 2020A1515010524).

Appendix A. Supplementary data

Supplementary data to this article can be found online at https://doi.org/10.1016/j.jinorgbio.2022.111977.

References

[1] M. Kanapathipillai, A. Brock, D.E. Ingber, Nanoparticle targeting of anti-cancer drugs that alter intracellular signaling or influence the tumor microenvironment, Adv. Drug Deliv. Rev. 79-80 (2014) 107–118.
[2] I.J. Fidler, Critical determinants of metastasis, Semin. Cancer Biol. 12 (2002) 89–96.
[3] B. Rosenberg, L. Vancamp, J.E. Trosko, V.H. Mansour, Platinum compounds: a new class of potent antitumour agents, Nature 222 (1969) 385–386.
[4] F.P.T. Harmers, W.H. Gispen, J.P. Neijt, Neurotoxic side-effects of cisplatin, Eur. J. Cancer 27 (1991) 372–376.
[5] S. Ghosh, Cisplatin: the first metal based anticancer drug, Bioorg. Chem. 88 (2019), 102925.
[6] A. Calls, A. Torres-Espin, X. Navarro, V.J. Yuste, E. Udina, J. Brun, Cisplatin-induced peripheral neuropathy is associated with neuronal senescence-like response, Neuro-Oncology 23 (2021) 88–99.
[7] J. Herrmann, Adverse cardiac effects of cancer therapies: cardiotoxicity and arrhythmia, Nat. Rev. Cardiol. 17 (2020) 474–502.
[8] C. Donohoe, M.O. Senge, L.G. Arnaut, L.C. Gomes-da-Silva, Cell death in photodynamic therapy: from oxidative stress to anti-tumor immunity, Biochim. Biophys. Acta Rev. Cancer. 1872 (2019), 188308.

[9] X.S. Li, J.F. Lovell, J. Yoon, X.Y. Chen, Clinical development and potential of photothermal and photodynamic therapies for cancer, Nat. Rev. Clin. Oncol. 17 (2020) 657–674.
[10] Z.J. Zhou, L. Zhang, Z.R. Zhang, Z.M. Liu, Advances in photosensitizer-related design for photodynamic therapy, Asian, J. Pharm. Sci. 16 (2021) 668–686.
[11] N.A. Smith, P.J. Sadler, Photoactivatable metal complexes: from theory to applications in biotechnology and medicine, Philos. Trans. A Math. Phys. Eng. Sci. 371 (1995), 20120519.
[12] C. Donohoe, M.O. Senge, L.G. Arnaut, L.C. Gomes-da-Silva, Cell death in photodynamic therapy: from oxidative stress to anti-tumor immunity, Biochim. Biophys. Acta Rev. Cancer 1872 (2019), 188308.
[13] R. Alzeibak, T.A. Mishchenko, N.Y. Shilyagina, I.V. Balalaeva, M.V. Vedunova, D. V. Krysko, Targeting immunogenic cancer cell death by photodynamic therapy: past, present and future, J. Immunother. Cancer. 9 (2021), e001926.
[14] H.W. Zhang, L. Tian, R.X. Xiao, Y. Zhou, Y.Y. Zhang, J. Hao, Y.J. Liu, J.P. Wang, Anticancer effect evaluation in vitro and in vivo of iridium(III) polypyridyl complexes targeting DNA and mitochondria, Bioorg. Chem. 115 (2021), 105290.
[15] J. Hao, H.W. Zhang, L. Tian, L.L. Yang, Y. Zhou, Y.Y. Zhang, Y.J. Liu, D.G. Xing, Evaluation of anticancer effects in vitro of new iridium(III) complexes targeting the mitochondria, J. Inorg. Biochem. 221 (2021), 111465.
[16] Y.H. Yuan, C.L. Shi, X.Y. Wu, W.L. Li, C.X. Huang, L.L. Liang, J. Chen, Y. Wang, Y. J. Liu, Synthesis and anticancer activity in vitro and in vivo evaluation of iridium (III) complexes on mouse melanoma B16 cells, J. Inorg. Biochem. 232 (2022), 111820.
[17] Y. Zhou, L. Bai, L. Tian, L.L. Yang, H.W. Zhang, Y.Y. Zhang, J. Hao, Y.Y. Gu, Y. J. Liu, Iridium (III)-BBIP complexes induce apoptosis via PI3K/AKT/mTOR pathway and inhibit A549 lung tumor growth in vivo, J. Inorg. Biochem. 23 (2021), 111550.
[18] Y.Y. Zhang, Y. Zhou, H.W. Zhang, L. Tian, J. Hao, Y.H. Yuan, W.L. Li, Y.J. Liu, DNA binding and evaluation of anticancer activity in vitro and in vivo of iridium(III) polypyridyl complexes, J. Inorg. Biochem. 224 (2021), 111580.
[19] C. Huang, C. Liang, T. Sadhukhan, S. Banerjee, Z.X. Fan, T.X. Li, Z.L. Zhu, P. Y. Zhang, K. Raghavachari, H.Y. Huang, In vitro and in vivo photocatalytic cancer therapy with biocompatible iridium (III) photocatalysts, Angew. Chem. Int. Ed. Eng. 60 (2021) 9474–9479.
[20] J.C. Shen, J. Karges, K. Xiong, Y. Chen, L.N. Ji, H. Chao, Cancer cell membrane camouflaged iridium complexes functionalized black-titanium nanoparticles for hierarchical-targeted synergistic NIR-II photothermal and sonodynamic therapy, Biomaterials. 275 (2021), 120979.
[21] H. Wu, Q. Jiang, K.Y. Luo, C.P. Zhu, M.M. Xie, S.G. Wang, Z.W. Fei, J.L. Zhao, Synthesis of iridium-based nanocomposite with catalase activity for cancer phototherapy, J. Nanobiotechnol. 19 (2021) 203.
[22] L. Markova, V. Novohradsky, J. Kasparkova, J. Ruiz, V. Brabec, Dipyridophenazine iridium (III) complex as a phototoxic cancer stem cell selective, mitochondria targeting agent, Chem. Biol. Interact. 360 (2022), 109955.
[23] C. Lee, J.S. Nam, C.G. Lee, M. Park, C.M. Yoo, H.W. Rhee, J.K. Seo, T.H. Kwon, Analysing the mechanism of mitochondrial oxidation-induced cell death using a multifunctional iridium (III) photosensitiser, Nat. Commun. 12 (2021) 26.
[24] Z.X. Fan, Y. Rong, T. Sadhukhan, S. Liang, W.Q. Li, Z.X. Yuan, Z.L. Zhu, S.W. Guo, S.M. Ji, J.Q. Wang, R. Kushwaha, S. Banerjee, K. Raghavachari, H.Y. Huang, Single-cell quantification of a highly biocompatible dinuclear iridium (III) complex for photocatalytic cancer therapy, Angew. Chem. Int. Ed. Eng. 61 (2022), e202202098.
[25] K. Xiong, Y. Zhou, X.L. Lin, J.F. Kou, M.W. Lin, R.L. Guan, Y. Chen, L.N. Ji, H. Chao, Cyclometalated iridium (III) complexes as mitochondria-targeting photosensitizers against cisplatin-resistant cells, Photochem. Photobiol. 98 (2022) 85–91.
[26] W.W. Qin, Z.Y. Pan, D.H. Cai, Y. Li, L. He, Cyclometalated iridium (III) complexes for mitochondria-targeted combined chemo-photodynamic therapy, Dalton Trans. 49 (2020) 3562–3569.
[27] X.Z. Li, J.G. Wu, L. Wang, C. He, L.Y. Chen, Y. Jiao, C.Y. Duan, Mitochondrial-DNA-targeted Ir^{III} -containing metallohelices with tunable photodynamic therapy efficacy in cancer cells, Angew. Chem. Int. Ed. Eng. 59 (2020) 6420–6427.
[28] X. Wang, K. Song, Y. Deng, J. Liu, Q. Peng, X. Lao, J.Y. Xu, D. Wang, T.R. Shi, Y. H. Li, D. Deng, Y.Q. Miao, Benzothiazole-decorated iridium-based nanophotosensitizers for photodynamic therapy of cancer cells, Dalton Trans. 51 (2022) 3666–3675.
[29] Y. Li, K.N. Wang, L. He, L.N. Ji, Z.W. Mao, Synthesis, photophysical and anticancer properties of mitochondria-targeted phosphorescent cyclometalated iridium (III) N-heterocyclic carbene complexes, J. Inorg. Biochem. 205 (2020), 110976.
[30] N. Manav, M.Y. Lone, M.K. Raza, J. Chavda, S. Mori, I. Gupta, Luminescent iridium (III) dipyrrinato complexes: synthesis, X-ray structures, and DFT and photocytotoxicity studies of glycosylated derivatives, Dalton Trans. 51 (2022) 3849–3863.
[31] M. Redrado, A. Bened, I. Marzo, M.C. Gimeno, V. Fernández-Moreira, Dual emissive Ir (III) complexes for photodynamic therapy and bioimaging, Pharmaceutics 13 (2021) 1382.
[32] I. Echevarría, E. Zafon, S. Barrabés, M.Á. Martínez, S. Ramos-Gómez, N. Ortega, B. R. Manzano, F.A. Jalón, R. Quesada, G. Espino, A. Massaguer, Rational design of mitochondria targeted thiabendazole-based Ir (III) biscyclometalated complexes for a multimodal photodynamic therapy of cancer, J. Inorg. Biochem. 231 (2022), 111790.
[33] E. Zafon, I. Echevarría, S. Barrabés, B.R. Manzano, F.A. Jalón, A.M. Rodríguez, A. Massaguer, G. Espino, Photodynamic therapy with mitochondria-targeted biscyclometallated Ir (III) complexes. Multi-action mechanism and strong influence of the cyclometallating ligand, Dalton Trans. 51 (2021) 111–128.
[34] D.D. Clark, L. Sokloff, Basic Neurochemistry: Molecular, Cellular and Medical Aspects, Lippincott, Philadelphia, 1999.
[35] R.H. Garrett, C.M. Grisham, Biochemistry, Saunders College Publishing, Orlando, FL, 1999.
[36] R.A. Medina, G.I. Owen, Glucose transporters: expression, regulation and cancer, Biol. Res. 35 (2002) 9–26.
[37] F.Q. Zhao, A.F. Keating, Functional properties and genomics of glucose transporters, Curr. Genomics 8 (2007) 113–128.
[38] F. Nualart, M. Los Angeles García, R.A. Medina, G.I. Owen, Glucose transporters in sex steroid hormone related cancer, Curr. Vasc. Pharmacol. 7 (2009) 534–548.
[39] W. Ho-Tin Law, L.C.C. Lee, M.W. Louie, H.W. Liu, T.W.H. Ang, K.K.W. Lo, Phosphorescent cellular probes and uptake indicators derived from cyclometalated iridium(III) bipyridine complexes appended with a glucose or galactose entity, Inorg. Chem. 52 (2013) 13029–13041.
[40] S. Sprouse, K.A. King, P.J. Spellane, R.J. Watts, Photophysical effects of metal-carbon σ bonds in ortho-metalated complexes of Ir(III) and Rh(III), J. Am. Chem. Soc. 106 (1984) 6647–6653.
[41] T. Mosmann, Rapid colorimetric assay for cellular growth and survival: application to proliferation and cytotoxicity assays, J. Immunol. Methods 65 (1983) 55–63.
[42] J.N. Demas, G.A. Crosby, Measurement of photoluminescence quantum yields, Phys J. Chem. 75 (1971) 991–1024.
[43] D.T. Manallack, The acid-base profile of a contemporary set of drugs: implications for drug discovery, SAR QSAR Environ. Res. 20 (2009) 611–655.
[44] D.T. Manallack, The pKa distribution of drugs: application to drug discovery, Perspect, Med. Chem. 1 (2007) 25–38.
[45] N. Manav, M.Y. Lone, M.K. Raza, J. Chavda, S. Mori, I. Gupta, Luminescent iridium (III) dipyrrinato complexes: synthesis, X-ray structures, and DFT and photocytotoxicity studies of glycosylated derivatives, Dalton Trans. 51 (2022) 3849–3863.
[46] W.Y. Zhang, Q.Y. Yi, Y.J. Wang, F. Du, M. He, B. Tang, D. Wan, Y.J. Liu, H. L. Huang, Photoinduced anticancer activity studies of iridium (III) complexes targeting mitochondria and tubules, Eur. J. Med. Chem. 151 (2018) 568–584.
[47] C. Zhang, S.H. Lai, H.H. Yang, D.G. Xing, C.C. Zeng, B. Tang, D. Wan, Y.J. Liu, Photoinduced ROS regulation of apoptosis and mechanism studies of iridium (III) complex against SGC-7901 cells, RSC Adv. 7 (2017) 17752.
[48] W.P. Fan, P. Huang, X.Y. Chen, Overcoming the achilles' heel of photodynamic therapy, Chem. Soc. Rev. 45 (2016) 6488.
[49] W.A. Velema, W. Szymanski, B.L. Feringa, Photopharmacology: beyond proof of principle, Am. Chem. Soc. 136 (2014) 2178.
[50] W. Lv, Z. Zhang, K.Y. Zhang, H. Yang, S. Liu, A. Xu, S. Guo, Q. Zhao, W. Huang, A mitochondri-targeted photosensitizer showing improved photodynamic therapy effects under hypoxia, Angew. Chem. Int. Ed. 55 (2016) 9947–9951.
[51] P. Zhang, H. Huang, S. Banerjee, G.J. Clarkson, C. Ge, C. Imberti, P.J. Sadler, Nucleus-targeted organoiridium–albumin conjugate for photodynamic cancer therapy, Angew. Chem. Int. Ed. 58 (2019) 2350–2354.
[52] Y.Y. Zhang, W.D. Fei, H.W. Zhang, Y. Zhou, L. Tian, J. Hao, Y.H. Yuan, W.L. Li, Y. J. Liu, Increasing anticancer effect in vitro and vivo of liposome-encapsulated iridium(III) complexes on BEL-7402 cells, J. Inorg. Biochem. 225 (2021), 111622.
[53] N. Kordestani, H.M. Rudbari, A.R. Fernandes, L.R. Raposo, P.V. Baptista, D. Ferreira, Bella G. Gruno, R. Scopelliti, J.D. Braun, D.E. Herbert, O. Blacque, Antiproliferative activities of diimine-based mixed ligand copper(II) complexes, ACS Comb. Sci. 22 (2020) 89–99.
[54] M.R. Zanotelli, J. Zhang, C.A. Reinhart-King, Mechanoresponsive metabolism in cancer cell migration and metastasis, Cell Metab. 33 (2021) 1307–1321.
[55] J.E.N. Jonkman, J.A. Cathcart, F. Xu, M.E. Bartolini, J.E. Amon, K.M. Stevens, P. Colarusso, An introduction to the wound healing assay using live-cell microscopy, Cell Adhes. Migr. 8 (2014) 440–451.
[56] W.L. Ma, X.X. Ge, Z.S. Xu, S.M. Zhang, X.D. He, J.J. Li, X.R. Xia, X.B. Chen, Z. Liu, Theranostic lysosomal targeting anticancer and antimetastatic agents: half-sandwich iridium (III) rhodamine complexes, ACS Omega. 4 (2019) 15240–15248.
[57] M. Wang, R.J. Kaufman, Protein misfolding in the endoplasmic reticulum as a conduit to human disease, Nature. 529 (2016) 326–335.
[58] H. Hu, M.X. Tian, C. Ding, S.Q. Yu, The C/EBP homologous protein (CHOP) transcription factor functions in endoplasmic reticulum stress-induced apoptosis and microbial infection, Front. Immunol. 9 (2019) 3083.
[59] A.P. King, J.J. Wilson, Endoplasmic reticulum stress: an arising target for metal-based anticancer agents, Chem. Soc. Rev. 49 (2020) 8113–8136.
[60] J. Adler, Quantifying colocalization by correlation: the Pearson correlation coefficient is superior to the mander's overlap coefficient, I. Parmryd, Cytom. Part A 77A (2010) 733–742.
[61] F.M. Wei, S. Kuang, T.W. Rees, X.X. Liao, J.P. Liu, D.Q. Luo, J.Q. Wang, X.T. Zhang, L.N. Ji, H. Chao, Ruthenium (II) complexes coordinated to graphitic carbon nitride: oxygen self-sufficient photosensitizers which produce multiple ROS for photodynamic therapy in hypoxia, Biomaterials. 276 (2021), 121064.
[62] J. Tian, B.X. Huang, Z.P. Cui, P. Wang, S. Chen, G.L. Yang, W.A. Zhang, Mitochondria-targeting and ROS-sensitive smart nanoscale supramolecular organic framework for combinational amplified photodynamic therapy and chemotherapy, Acta Biomater. 130 (2021) 447–459.
[63] R.J. He, M. Cui, H. Lin, L. Zhao, J.Y. Wang, S.F. Chen, Z.W. Shao, Melatonin resists oxidative stress-induced apoptosis in nucleus pulposus cells, Life Sci. 199 (2018) 122–130.
[64] L. Haide, Inflammation, iron, energy failure, and oxidative stress in the pathogenesis of multiple sclerosis, Oxidative Med. Cell. Longev. 2015 (2015), 725370.

[65] L.J. Su, J.H. Zhang, H. Gomez, R. Murugan, X. Hong, D.X. Xu, F. Jiang, Z.Y. Peng, Reactive oxygen species-induced lipid peroxidation in apoptosis, autophagy, and ferroptosis, Oxidative Med. Cell. Longev. 13 (2019) 5080843.
[66] M.W. Park, H.W. Cha, J. Kim, J.H. Kim, H. Yang, S. Yoon, N. Boonpraman, S.S. Yi, I.D. Yoo, J.S. Moon, NOX4 promotes ferroptosis of astrocytes by oxidative stress-induced lipid peroxidation via the impairment of mitochondrial metabolism in Alzheimer's diseases, Redox Biol. 41 (2021), 101947.
[67] S.R. Pieczenik, J. Neustadt, Mitochondrial dysfunction and molecular pathways of disease, Exp. Mol. Pathol. 83 (2007) 84–92.
[68] I. Martínez-Reyes, L.P. Diebold, H. Kong, M. Schieber, H. Huang, C.T. Hensley, M. M. Mehta, T. Wang, J.H. Santos, R. Woychik, E. Dufour, J.N. Spelbrink, S. E. Weinberg, Y. Zhao, R.J. DeBerardinis, N.S. Chandel, TCA cycle and mitochondrial membrane potential are necessary for diverse biological functions, Mol. Cell 61 (2016) 199–209.
[69] K.G. Lyamzaev, A.V. Tokarchuk, A.A. Panteleeva, A.Y. Mulkidjanian, V. P. Skulachev, B.V. Chernyak, Induction of autophagy by depolarization of mitochondria, Autophagy. 14 (2018) 921–924.
[70] W. Li, J. Yang, L.H. Luo, M.S. Jiang, B. Qin, H. Yin, C.Q. Zhu, X.L. Yuan, J.L. Zhang, Z.Y. Luo, Y.Z. Du, Q.P. Li, Y. Lou, Y.Q. Qiu, J. You, Targeting photodynamic and photothermal therapy to the endoplasmic reticulum enhances immunogenic cancer cell death, Nat. Commun. 10 (2019) 3349.
[71] X.P. Duan, C. Chan, W.B. Lin, Nanoparticle-mediated immunogenic cell death enables and potentiates cancer immunotherapy, Angew. Chem. Int. Ed. Eng. 58 (2019) 670–680.
[72] T.S. Lau, L.K.Y. Chan, G.C.W. Man, C.H. Wong, J.H.S. Lee, S.F. Yim, T.H. Cheung, I. A.M. McNeish, J. Kwong, Paclitaxel induces immunogenic cell death in ovarian cancer via TLR4/IKK2/SNARE-dependent exocytosis, Cancer, Immunol. Res. 8 (2020) 1099–1111.
[73] J. Fucikova, P. Kralikova, A. Fialova, T. Brtnicky, L. Rob, J. Bartunkova, R. Spísek, Human tumor cells killed by anthracyclines induce a tumor-specific immune response, Cancer Res. 71 (2011) 4821–4833.
[74] L.J. Mah, A. El-Osta, T.C. Karagiannis, GammaH2AX: a sensitive molecular marker of DNA damage and repair, Leukemia. 2 (2010) 679–686.
[75] H.R. Guo, Y.J. Ouyang, J.Q. Wang, H.M. Cui, H.D. Deng, X.Y. Zhong, Z.J. Jian, H. Liu, J. Fang, Z.C. Zuo, X. Wang, L. Zhao, Y. Geng, P. Ouyang, H.Q. Tang, Cu-induced spermatogenesis disease is related to oxidative stress-mediated germ cell apoptosis and DNA damage, J. Hazard. Mater. 416 (2021), 125903.
[76] J. Krupinski, I. Ferrer, M. Barrachina, J.J. Secades, J. Mercadal, R. Lozano, CDP-choline reduces pro-caspase and cleaved caspase-3 expression, nuclear DNA fragmentation, and specific PARP-cleaved products of caspase activation following middle cerebral artery occlusion in the rat, Neuropharmacology. 42 (2002) 846–854.
[77] J. Matsuo, S. Haga, K. Hashimoto, T. Okubo, T. Ozawa, M. Ozaki, H. Yamaguchi, Activation of caspase-3 during chlamydia trachomatis-induced apoptosis at a late stage, Can. J. Microbiol. 65 (2019) 135–143.
[78] A. Bressenot, S. Marchal, L. Bezdetnaya, J. Garrier, F. Guillemin, F. Plénat, Assessment of apoptosis by immunohistochemistry to active caspase-3, active caspase-7, or cleaved PARP in monolayer cells and spheroid and subcutaneous xenografts of human carcinoma, J. Histochem. Cytochem. 57 (2009) 289–300.
[79] J.L. Yang, C.C. Pi, G.H. Wang, Inhibition of PI3K/Akt/mTOR pathway by apigenin induces apoptosis and autophagy in hepatocellular carcinoma cells, Biomed. Pharmacother. 103 (2018) 699–707.
[80] Q. Yang, W. Jiang, P. Hou, Emerging role of PI3K/AKT in tumor-related epigenetic regulation, Semin. Cancer Biol. 59 (2019) 112–124.